Integrated solar-driven hydrogen generation by pyrolysis and electrolysis coupled with carbon capture and Rankine cycle.

Linus Onwuemezie, Hamidreza Gohari Darabkhani, Mohammad Moghimi Ardekani

Department of Engineering, School of Digital, Technologies and Arts (DTA), Staffordshire University, Stoke-on-Trent, ST4 2DE, UK

** Corresponding Author email: h.g.darabkhani@staffs.ac.uk*

HIGHLIGHTS

- Innovative solar-driven pyrolysis systems are proposed for clean hydrogen generation.
- Desulphurisation of methane feedstock to minimise catalyst deactivation.
- The integrated systems include electrolysis and molten salt for thermal energy storage (TES)
- The hybrid system includes carbon capture and the use of recovered heat to generate electricity.
- Process simulation and sensitivity analysis for the study of reactions' parameters.

GRAPHICAL ABSTRACT

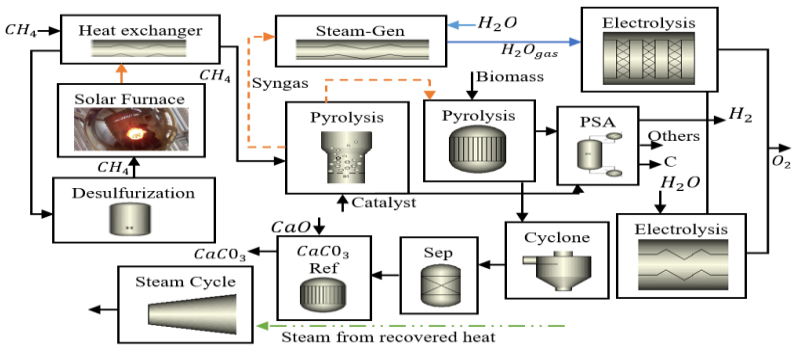

Keywords:
Concentrating Solar Power (CSP)
Methane and biomass pyrolysis
Thermolysis of sulphuric acid (H_2SO_4)
Electrolysis of water (H_2O)
Rankine cycle
CO_2 capture and carbon neutral

Nomenclature

Abbreviations and Symbols

%	Percentage
°C	Degrees Celsius
ΔH	Enthalpy
e^-	Electron
H^+	Proton
OH^-	Hydroxide
$m\mu$	Millimicron
n	Efficiency
μm	Micron
wt.%	Percentage by weight
AEC	Alkaline electrolyser cell
CCUS	Carbon capture and utilisation and storage
CI	Conventional inert
CMD	Catalytic methane decomposition
CO_2e	Carbon emission equivalent
CSP	Concentrating Solar Power
DNI	Direct normal irradiance
EAOC	Equivalent annual operating cost
H_2SO_4	Sulphuric acid
HP	Hydrocarbon pyrolysis
HTF	Heat Transfer Fluids
HX	Heat exchangers
IMBP	Integrated methane and biomass pyrolysis
IPCC	Intergovernmental Panel on Climate Change
kg/hr	Kilo gram per hour
$kmol/hr$	Kilo mole per hour
kW	Kilowatt
KNO_3	Potassium nitrate
kta	Kilo Tons per Annum
m^2	square metre
m/s	Metre per second
MENA	The Middle East and North Africa
MW	Megawatt
Mta	Mega Tons per Annum
$NaNO_3$	Sodium nitrate
NC	Non-conventional
NREL	National Renewable Energy Laboratory
NRTL	Non-Random Two-Liquid
PEMEC	Proton exchange membrane electrolyser cell
PMEW	Pyrolysis of methane and electrolysis of water
PSD	Particle size distribution
S/C	Steam carbon ratio
SAM	System Advisor Model
SE-CL	Sorption Enhanced–Chemical Looping
SMR	Steam methane reforming
SO_2	Sulphur dioxide
SOEC	Solid oxide electrolyser cell
TES	Thermal energy storage
WGS	Water gas shift
W/m^2	Watt per square metre

ABSTRACT

Reduction of carbon emissions from conventional gray Hydrogen (H_2) production is a promising option in moving towards much greener H_2 generation. To minimise carbon emissions and improve plants' efficiencies of conventional gray H_2 production, this study focused on process simulation of hybrid CSP, catalytic Methane (CH_4) and biomass pyrolysis and Water (H_2O) electrolysis plants with 1000°C HTF output temperature. This integrated system differs from current pyrolysis and electrolysis technologies for H_2 production because of the involvement of CSP as a thermal energy source; the use of part of recovered heat from the reactor to power downstream units including thermolysis of Sulphuric Acid (H_2SO_4) and steam generation for both H_2O electrolysis and Rankine cycle; the use of H_2O as a reaction media and carbon looping to promote biomass decomposition; anodic oxidation of SO_2 in AEC to promote hydrogen evolution reaction. In that regard, CSP systems were modelled and simulated in SAM and MATLAB software. The output result of the simulated CSP system got exported to the Simulink to feed simulated CH_4 and biomass pyrolysis coupled with TES and Rankine cycle from Aspen plus. In addition, simulated thermal disassociation of H_2SO_4, electrolysis of H_2O with SOEC and AEC from Aspen plus was also exported to the Simulink to feed the CSP system. Both integrated systems were fed with CH_4 as the working fluid of the solar furnace. About $1.7/kg is estimated to be a H_2 selling price for simulated pyrolysis of CH_4 and biomass plant which is cheaper than SMR with a CCS system. While between 4.6 - 10.48 is also estimated to be a H_2 selling price for another simulated CH_4 pyrolysis and H_2O electrolysis. Just like existing CSP systems for electricity generation, both simulated hybrid systems generate electricity for up to 200 minutes in the absence of the Sun. Similar to SMR with a CCS system, CO_2 by-product from biomass pyrolysis was captured. Due to coking issues related to catalytic pyrolysis, noncatalytic pyrolysis of CH_4 was investigated. Results of the research work show that a return on investment within a period of 6 years is possible with the adoption of these new innovative technologies while reducing carbon footprints in H_2 generation plants.

1.0 Introduction

An increase in energy demand has increased carbon emissions into the atmosphere because of the utilisation of fossil fuels in an absence of carbon capture and storage (CCS). In addition, the amount of solid waste disposed into the environment has increased due to rapid urbanisation. Thus, energy transition from fossil fuels to eco-friendly fuels, and recycling of biomass and other environmental wastes to produce energy is necessary to limit temperature rise above 2°C (degrees Celsius) as set by IPCC [1]. Hydrogen (H_2) fuel from renewable and fossil fuels resources equipped with carbon capture, utilisation and storage (CCUS) can be considered as the primary energy carrier of the future to supplement fossil fuels as such that water (H_2O) is one of the by-products via a fuel cell application [2]. Unlike fossil fuels that occur in nature, Hydrogen (H_2) is a flammable, odourless and non-toxic substance that can be found on the earth with other elements such as organic compounds and H_2O. Molecular hydrogen [$H_2(g)$] was first discovered by Paracelsus in 1493–1541. While well-known H_2 gas was discovered by Henry Cavendish in 1766 [3]. Reforming, pyrolysis, gasification, water (H_2O) splitting, biological and thermochemical processes are well-established and emerging technologies for extracting molecular H_2 from other elements. Despite the Global share of hydrocarbon reforming methods of producing H_2, methane (CH_4) and biomass pyrolysis offer several advantages like absences of CO_2 by-product in CH_4 pyrolysis, reduction of environmental waste and generation of other valuable products in biomass pyrolysis. Nonetheless, thermochemical and photochemical H_2O splitting processes of H_2 generation are considered more eco-friendly methods of H_2 production [4]. Although, pyrolysis and renewable sources like electrolysis methods of producing H_2 are effective steps forward towards net-zero carbon emissions for sustainable development.

Pyrolysis involves the use of a high-temperature thermal energy source (>500°C) to transform liquid gas and solid fuel into synthetic gas or gaseous fuels in the absence of partial oxidation. Many researchers have reported that a temperature of approximately 1200°C is required for CH_4 decomposition without a catalyst present in the reactor [5]. A study by *Riley, et al.* [6] reported that hydrocarbon pyrolysis (HP) requires a catalyst for continuous steady-state operation in the fluidised bed decomposer to decrease the activation energy and mitigate kinetic limitations associated with noncatalytic pyrolysis. It was found that the aforementioned technology (HP) requires less activation energy and is cheaper than reforming processes of H_2 generation because of the absence of water gas shift (WGS) units and selling off another end product like carbon [6]. Nonetheless, *Msheik, et al.* [7] mentioned that a catalyst with less coke formation because of carbon deposition on the active site and a desulphurisation unit is very important to reduce early catalyst deactivation. Thus, *Geng, et al.* [5] maintained that the use of metallic catalysts such as nickel (Ni), iron (Fe) and Cobalt (Co) supports offers several advantages like less activation energy. For example, >58% of CH_4 conversion efficiency can be achieved with the use of a Ni-based catalyst compared with Fe and Co with an operating temperature below 750°C [5]. Nevertheless, fast catalyst deactivation and toxicity are drawbacks of such catalysts. Despite the benefits of both Fe and Co over Ni catalysts, coking remains one of the drawbacks of all the above-mentioned catalysts as catalyst deformation occurs in every complete cycle [8]. Not long ago, an effort to mitigate coking issues related to catalytic methane decomposition (CMD) was investigated by *Abánades, et al.* [8]. From the investigated work,

it was found that carbon deposited on the metal catalyst active site can be removed by the integration of both steam and oxygen (O_2) cycles to produce carbon monoxide (CO), CO_2 and more H_2 at moderate operating temperatures. Coke removal from steam regeneration with Ni/SO_2 catalyst was lower but more effective than air regeneration. Despite the removal of coking from the catalyst, CO_2 by-products and coking over a long period remain another disadvantage of such mitigation approaches. The use of carbonaceous catalysts to minimise coking issues and eliminate CO_2 by-products has also been studied for CH_4 pyrolysis. Nonetheless, Ni/Al_2O_3 catalyst has been widely recognised for greater thermal stability, resistance to carbon deposition of the active site and high conversion and reduction temperature of 700°C in methane pyrolysis and dry reforming of methane [9]. Despite lower conversion efficiency in comparison with metallic catalysts because of morphology modification, tolerance to impurities, absence of CO_2 by-products, contamination and regeneration were found to be advantages of such catalysts [10]. Therefore, to mitigate catalytic CH_4 pyrolysis limitations and drawbacks like carbon emission, noncatalytic CH_4 pyrolysis is needed with the integration of solar energy to provide the required thermal energy for CH_4 decomposition [7]. CH_4 pyrolysis which differs from the gasification process is displayed in Fig. 1. While Eqs 1 and 2 represent the desulphurisation and CH_4 cracking process of H_2 and carbon production.

$$H_2 + S \leftrightarrow H_2S \quad \Delta H^0_{298} \tag{1}$$

$$CH_4 \leftrightarrow 2H_2 + C \quad \Delta H^0_{298} = 74.8 kJ/mol \tag{2}$$

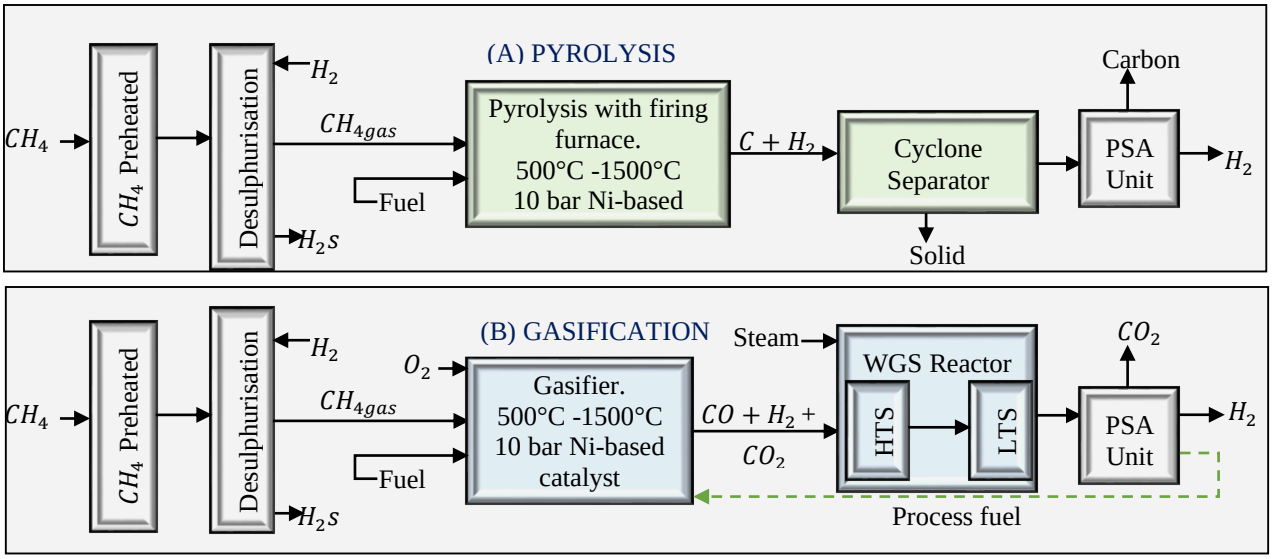

Figure 1: A schematic flow diagram of catalytic (A) pyrolysis and (B) gasification processes for H_2 production

Pyrolysis and gasification are the 2 main thermochemical processes of transforming biomass into syngas. Bio-crude, solid charcoal and synthetic gases as by-products can be produced by heating biomass feed between 500 – 1400°C, with the presence and absence of oxidising agents as displayed in Fig. 2 [11]. Biomass pyrolysis differs from biomass gasification in that syngas and other by-products as mentioned are produced in a non-oxidising environment except H_2O. *Uddin, et al.* [12] stated that biomass pyrolysis of producing syngas includes drying to remove moisture, grinding, decomposition in the pyrolysis first reactor and thermal reduction. While *Nikolaidis & Poullikkas.* [13] maintained that a higher biomass conversion rate can be achieved in biomass catalytic pyrolysis at 527°C temperature and 5 bar pressure. Unlike coal gasification to produce H_2, biomass is renewable as its sources such as crops can be grown after each harvest. In addition, pyrolysis is regarded as a promising pathway for the treatment of hazardous waste like sewage sludge [14]. In contrast, exergy losses in biomass gasification are much greater compared to coal gasification because of a high O_2 content (about 40 wt.%). Nonetheless, the use of feedstocks with less acidity, high volatile matter (a mixture of $CO, CO_2, H_2O_{gas}, CH_4$, and H_2) and less ash content; good oxidising stability and deoxygenation promoted catalyst with up to 30wt.% catalyst concentration has been widely studied as a possible approach to mitigate the aforementioned drawbacks of biomass pyrolysis. For instance, *Luna-Murillo, et al.* [15] reported that the use of a well-known petroleum catalyst (zeolite socony mobil–5 (ZSM-5)) in biomass pyrolysis has shown tremendous performance improvement in deoxygenation. Yet, low carbon yield and deactivation of catalysts because of coking remain a major challenge. Most recently, *Ellison & Boldor.* [16] carried out a study by impregnating a montmorillonite K10 with 10% Fe loadings to reduce catalyst degradation and reported less coke formation with the absence of long-term performance analysis of the stability and degradation after regeneration. Nevertheless, a drop in liquid syngas concentration because of the instability of carboxylic acids and aldehydes was also recorded [16]. Findings show that catalytic biomass pyrolysis drawbacks do follow the same mitigation trend mentioned in catalytic CH_4 pyrolysis. Thus, the incorporation of non-polluting thermal energy sources, catalysts with less deactivation and the absence of catalysts are required to overcome the

aforementioned limitations and drawbacks. Ash (inorganic), carbon (C), hydrogen (H_2), methane (CH_4), olefin (ethene (ethylene "C_2H_4") and propene (propylene "C_3H_6")), nitrogen (N_2), chlorine (Cl_2), sulphur (S), oxygen (O_2) and alkali metal content are the ultimate composition of biomass. While fixed carbon, volatile matters, ash and H_2O are the proximate and biochemical composition of biomass. Equations for calculating and estimating CH_4 conversion, H_2 yield (%) and CO_2 capture efficiencies are represented in Eqs 3 – 5.

$$CH_4\ conversion\ = \left[\frac{n_{CH_{4,in}} - n_{CH_{4,out}}}{n_{CH_{4,in}}}\right] * [100]\% \quad (3)$$

$$H_2\ yield\ |\%| = \left[\frac{n_{H_{2,out}}}{n_{H_{2,in}}}\right] * [100] \quad (4)$$

$$CO_2\ capture\ = \left[\frac{n_{CH_{4,in}} - n_{CH_{4,out}} - n_{CO_{2,in}} - n_{CO_{2,out}}}{n_{CH_{4,in}}}\right] * [100]\% \quad (5)$$

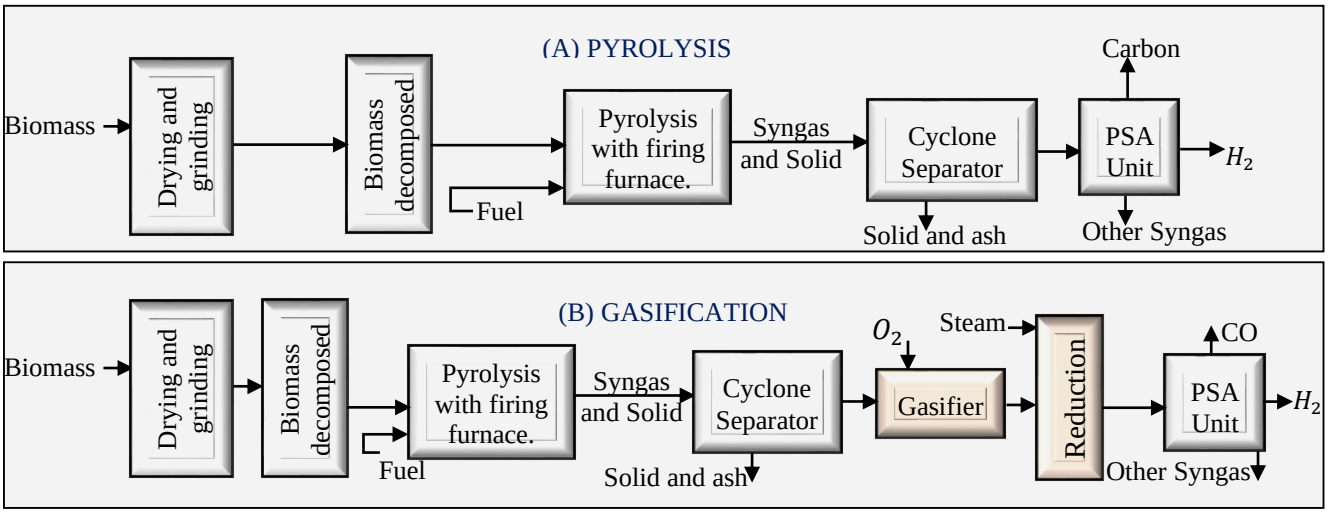

Figure 2: A schematic flow diagram of noncatalytic (A) pyrolysis and (B) gasification processes for H_2 production

Electrolysis of H_2O generate H_2 in the cathode side and O_2 in the anode side as by-products through the electrochemical splitting of H_2O by the passage of electricity between 2 separated electrodes. This process is endothermic because of the involvement of ohmic heating (joule heating) [17]. Alkaline electrolyser cell (AEC), solid oxide electrolyser cell (SOEC) and proton exchange membrane electrolyser cell (PEMEC) are the 3 main types of electrolysis of H_2O technologies. Each of these technologies for the production of H_2 has different and related limitations and utilises different operating temperatures, electrolytes and ionic agents (OH^-, H^+, O^{2-}). For instance, electrolyte resistance and electrode surface damage resulting in large ohmic loss was reported as one of the major impacts of H_2 and O_2 bubbles deposit on the electrodes during the electrolysis of H_2O molecule in AEC [17]. Thus, the transition to zero-gap cell configuration (bipolar with less ohmic loss) and kinetics performance analysis of the electrodes in H_2 and O_2 evolution reactions to minimise carbonation performance can enhance AEC efficiency and service life [17]. In addition, the use of alloy metals with good hydrophilicity, microstructure, surface area and large surface roughness to accelerate the speed of O_2 generation can also enhance AEC efficiency [17]. For example, the use of porous Raney Ni-based electrode impregnated with Fe and cobalt oxide (Co_3O_4) powder support; synthetic Ni-Mo with $NiMoO_4$ powder support; transition to noble metal-based electrodes; use of an impregnated alkali organic separator with electrode embedded onto it in a zero-gap assembly [18]. However, *Bodner, et al.* [19] assumed that such mitigation approaches like a complex configuration design of bipolar may lead to leakage and other issues in the AEC stack. Rather than the need for a complex bipolar design of AEC, *Díaz-Abad, et al.* [20] review shows that the application of the Westinghouse cycle with transitional or noble metals electrodes as represented in Eqs 11-13 can improve the efficiency and service life of AEC. For instance, *Zhao, et al.* [21] investigated Fe–N-doped carbon cladding catalyst for the improvement of anodic oxidation. It was found that excellent sulphur dioxide (SO_2) electrochemical oxidation is possible because of good stability and fast transport substrates in the electrolysis of H_2O. The Westinghouse cycle involves the thermal decomposition of sulphuric acid (H_2SO_4) and the electrolysis of SO_2.

Unlike AEC, SOEC consists of $oxygen - ion$ ($O - ion$) and $hydrogen$ ($H - ion$) conducting SOECs and uses steam as substrate. In the $O - ion$ SOECs, the infeed (H_2O_{gas}) take place in the anode side to produce O_2, proton (H^+) and electron (e^-). In $proton - ion$ SOECs, another infeed takes place in the cathode side to generate H_2 and $O - ion$ during the electrochemical reactions. O_2 combines with $O - ion$ after oxidation as it travels through the electrolyte in $proton - ion$ SOECs. Process simulation of both $O - ion$ and $H - ion$ SOECs shows that higher selectivity occurs at operating temperatures lower than 776.85°C in $H - ion$ SOECs. Whereas high pressure and temperature greater than 776.85°C favours $O - ion$

SOECs. However, a reduction in ohmic overpotential is expected with more temperature increase [22]. Electrodes and electrolyte degradation as a result of poor mechanical strength, thermal and chemical stabilities and polarisation resistance are reported as drawbacks of the SOEC system [23]. Nonetheless, hybridisation that allows the use of Ni-based yttria-stabilized zirconia (YSZ) electrode for the anode, fabricated materials like $La\ Sr\ FeO_3$ (LSCF) for cathode and gadolinium-doped ceria (CGO/GDC) electrolyte have been viewed as a possible approach to mitigate such drawbacks. Although, thinning of Ni-YSZ electrode of the SOEC system because of the porosity increase in the inside active layers remains an unsolved issue [24]. A short while ago, *Im-orb, et al.* [25] study illustrated that a mixture of H_2O_{gas} and part of H_2 (10 Vol%) from H_2 separator as the reactant feed to the cathode cells; feeding of minimal volume of O_2 from O_2 separator to the anode cells to maintain good thermal management of the cells can reduce the oxidation of Ni-YSZ electrode. Still, lanthanum strontium manganite (LSM) is regarded as the reference material for the configuration of SOECs because it exhibits good stability at an elevated operating temperature despite electrodes and electrolyte degradation issues [23]. Electricity dependant, high cost due to the use of steam as substrate feed and short service life are still drawbacks of H_2O electrolysis. Therefore, the use of recovered thermal energy in existing H_2 generation plants to produce steam and denoised H_2O for SOEC and AEC can alleviate the overall cost as *Nami, et al.* [26] mentioned that the use of free steam will make SOEC cheaper in the future. In addition, oxidation of SO_2 in anode chamber can also improve the overall efficiency of AEC. Eqs 6 and 7 are chemical reactions of H_2 conducting SOECs. While the overall reaction of electrolysis of H_2O for H_2 and O_2 generation is represented in Eq 8.

$$2H^+ + 2e^- \leftrightarrow O^{2-} + H_2\ (Cathode) \tag{6}$$

$$H_2O \leftrightarrow 2H^+ + \frac{1}{2}O_2 + 2e^-\ (Anode) \tag{7}$$

$$H_2O + electricity \leftrightarrow H_2 + 0.5O_2 \tag{8}$$

Thermolysis of H_2O that uses direct solar thermal energy to disassociate H_2O molecule into H_2 and O_2 gases at a temperature between 500 – 2000°C have been suggested as an alternative to both fossil fuels and electrolysis methods of H_2 generation. Zn/ZnO redox reactions through endothermic and exothermic hydrolysis reactions have been proposed for the design of H_2O thermolysis of H_2 generation system [27]. However, the use of extreme temperature to generate H_2 limit the widespread of H_2O thermolysis through ZnO redox reaction because of difficulties in material selection for the system design. Thus, thermolysis of H_2SO_4 has attracted attention as such that at a reaction temperature of 850°C, H_2SO_4 can be disassociated into H_2O, SO_2 and $0.5O_2$. Followed by the application of H_2O electrolysis to oxidise SO_2 in anode chamber and generate H_2 in the cathode side at cell voltage and temperature of 0.158V and 100°C [28]. Recovered heat from advanced nuclear reactors and concentrating sunlight to split H_2SO_4 for H_2O electrolysis has been viewed as promising option for AEC. Eqs 9 and 10 represent chemical reactions of H_2O thermolysis with the use of ZnO and H_2O as substrates. While Eqs 11-13 are chemical reactions of H_2SO_4 process for H_2 generation.

$$ZnO \leftrightarrow Zn + \frac{1}{2}O_2 \tag{9}$$

$$Zn + H_2O \leftrightarrow Zn0 + H_2 \tag{10}$$

$$H_2SO_4 \rightarrow H_2O + SO_2 + \frac{1}{2}O_2 \tag{11}$$

$$SO_2 + 2H_2O + electricity \rightarrow H_2SO_4 + 2H^+ + 2e^- \tag{12}$$

$$2H^+ + 2e^- \rightarrow H_2 \tag{13}$$

Concentrating solar power (CSP) which differs from Photovoltaic (PV) technology converts solar energy from the sun to thermal and electrical energy. CSP technologies include four main types: parabolic dishes (PD), power tower (PT), parabolic trough collectors (PTC) and linear Fresnel collectors (LFC). In a CSP system, a receiver which has the same working principle as the heat exchanger absorbs reflected solar energy from mirrors and exchanges it with the working fluid to generate thermal energy. Despite the high cost of CSP systems, energy generation during peak periods by the use of thermal energy storage (TES) is one of the greatest advantages compared to PV systems in large-scale plants [29]. Thus, CSP installation in MENA (the Middle East and North Africa) regions that experiences more sunshine during the day has been reported as the best approach for efficiency improvement [30]. For instance, *Azouzoute, et al.* [30] reported high electricity output and lower electricity cost of CSP systems located in MENA regions in contrast to the one installed in Spain. Nonetheless, *Labordena, et al.* [31] maintained that a good transmission line is required in developing countries to achieve fossil fuels energy transition to renewable through CSP systems. Considering the limitations of pyrolysis cracking of liquid and solid fuels, thermolysis of H_2SO_4 and electrolysis of SO_2 to produce H_2, incorporation of CSP system and improvement of electricity transmission lines to minimise losses have been viewed as the way forward to alleviate some of these aforementioned drawbacks.

Due to greenhouse gas emissions related to conventional fossil fuels processes of H_2 production in referenced to the above literature studies, eco-friendly pyrolysis and electrolysis technologies are urgently needed for substitutes. Indeed, fossil fuels are burnt in conventional plants to provide the required thermal energy for the endothermic cracking of CH_4 and biomass, generation of steam and electricity; consequently, releasing CO_2 into the atmosphere as a by-product. In that regard, researchers must overcome unaddressed limitations and restrictions reported in the literature and promote the use of non-polluting thermal energy sources and the improvement of H_2 plants' efficiencies. Thus, this work aimed to develop integrated H_2 generation technologies that use a CSP system as an energy source for feedstocks decomposition; application of waste energy recovering

to power downstream units of the same integrated system; capture of CO_2 by-product from biomass pyrolysis of the integrated system; enhancement of catalytic activities in both hydrogen and oxygen evolution reactions of the integrated system to address some of the reported drawbacks of current H_2 production processes. This study investigates and implements the below points in a process simulation to promote the feasibility of carbon neutrality and efficiency improvement in both fossil fuels and renewable sources of H_2 production:

i) integration of catalytic pyrolysis of CH_4 and biomass pyrolysis coupled with carbon capture for efficiency improvement;

ii) carbon looping in biomass pyrolysis to promote fast decomposition of biomass feed without the need for catalysts;

iii) integration of catalytic CH_4 pyrolysis, thermolysis of H_2SO_4 and electrolysis of H_2O (AEC with anodic oxidation of SO_2 and SOEC) for efficiency improvement;

iv) utilising concentrating solar power (CSP) to drive the endothermic cracking of CH_4, biomass wood and H_2SO_4 feeds with CH_4 as the working fluid;

v) utilising recovered thermal energy to heat a molten salt and incorporating thermal energy storage (TES) in a Rankine cycle;

vi) hybrid noncatalytic CH_4 pyrolysis, thermolysis of H_2SO_4 and H_2O electrolysis (AEC with anodic oxidation of SO_2 and SOEC) to eliminate catalyst deactivation associated with catalytic CH_4 pyrolysis over a while.

The scope of this study is divided into two separate parts: 1) Integration of biomass pyrolysis into CH_4 pyrolysis and Rankine cycle; 2) Integration of H_2O electrolysis into CH_4 pyrolysis and Rankine cycle. Both hybrid systems use a CSP system as a thermal energy source for feedstock decomposition. Simplified block flow diagrams of both integrated models are displayed in Fig. 3. In Fig. 3, the first integrated plant comprise of CH_4 pyrolysis (A), biomass pyrolysis (B) and Rankine cycle (D). While the second hybrid plant include CH_4 pyrolysis (A), thermolysis of H_2SO_4, and H_2O electrolysis (C) and Rankine cycle (D).

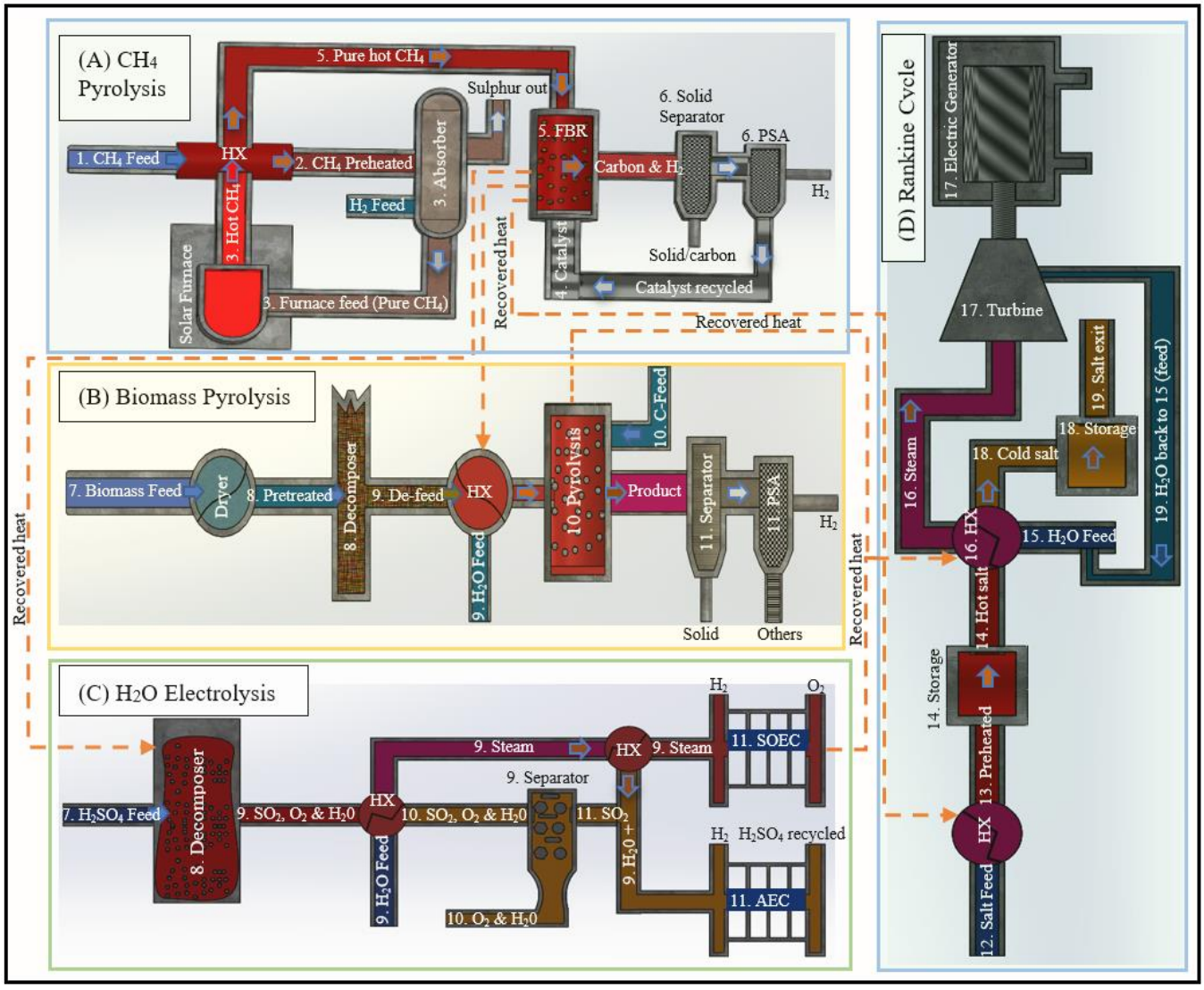

Figure 3: Catalytic pyrolysis of CH_4, biomass pyrolysis, H_2O electrolysis and Rankine cycle for H_2 and electricity generation.

2.0 Material and Simulation Method

In this study, CH_4, biomass (wood), H_2SO_4, and H_2O were selected materials used to study pyrolysis, thermolysis and electrochemical splitting of H_2O processes to generate H_2 and other valuable products. $Ni+$ dolomite was reduced to 330 microns (μm) mean size and mixed with CH_4 feedstock in the FBR to investigate catalytic and noncatalytic CH_4 pyrolysis mechanisms of both simulated systems. This approach substitutes adding about $5g\ \gamma - Al_2O_3$ into dissolved 15wt% $Ni(NO_3)_2.6H_2O$ loading in a distilled H_2O to form Ni/Al_2O_3, then followed by drying and thermal calcination [9]. $Ni/$dolomite was considered over Ni/Al_2O_3 catalyst for these integrated simulated plants because of the absence of sulphur deposit on the catalyst active site with desulphurised feedstock [32]. On conventional inert (CI) substream, Rosin–Rammler–Sperling–Bennet (RRSB) distribution function type with the upper and lower limit of 1 – 35 microns (μm) of logarithmic mesh particle size distribution (PSD) were applied during the preparation of the $Ni/$dolomite catalyst feed.

For the analysis of the process simulation of the integrated H_2 generation technologies, two simulation case scenarios are involved. While reaction parameters of biomass feed taken from published data are represented in Table 1.

- Case 1 is modelling and simulating CSP plants as a crucial step in generating the required thermal energy to drive endothermic cracking of CH_4, biomass and H_2SO_4 for H_2 generation.
- Case 2 is modelling and simulating hybrid catalytic methane (CH_4) and biomass pyrolysis (CMBP); catalytic CH_4 pyrolysis and electrolysis processes and noncatalytic methane (CH_4) and water electrolysis (NCMWE) of H_2 generation coupled with TES in a Rankine cycle. Two of these hybrid plants are then incorporated into the CSP system.

Table 1: Reaction parameters considered for the process simulation of lignocellulose biomass pyrolysis

Proximate analysis (wt%)					Reaction parameters taken from [33] [34] (wt%)						
Moisture	Fixed carbon	Volatile	Ash		Carbon monoxide (CO)	Hydrogen (H_2)	Carbon dioxide (CO_2)	Methane (CH_4)	Tar ($C_4H_6O_6$)	Chlorine (H_2O)	Ash
0	0.34	0.75	1.0		0.099	0.08	0.077	0.004	0.3931	0.26	0.0869

2.1 Concentrating Solar Power System (CSPS) Modelling and Simulation

SAM-NREL (System Advisory Model-National Renewable Energy Laboratory) tool along with MATLAB software were used for modelling and simulating parabolic trough collectors (PTC) CSP system. In the SAM environment, the listed input parameters in Table 2 were considered for purpose of modelling. As the project focuses on having a CSP system that operates at a higher temperature and the integrated system in one environment, the algorithm of the CSP system from SAM was exported to MATLAB for modification and inclusion of some useful parameters. Simulation of solar field parameters, collector and receiver orientation of the CSP was carried out in MATLAB and the result which is input to Simulink was saved in the MATLAB workspace.

Table 2: CSP plant specifications and configurations

Parameters	Value	Parameters	Value
Solar Field Parameters		**Solar Field Design Point and Land**	
Solar multiple	2.6	Actual number of loop	235-271
Design point DNI	950 W/m^2	Total aperture reflective area	1233280 m
Row spacing	15m	Solar field area	762 acres
Wind stow speed	25 m/s	Total land area	10687 acres
HTP pump efficiency	0.85	Non-solar field land area multiplier	1.4
Number of field subsection	2	**Collector and Receiver**	
Heat Transfer Fluid and Collector Orientation		Reflective aperture area	656 m^2
Loop intake HTF temperature	350°C	Aperture width, total structure	6m
Loop exit HTF temperature	958 – 1000°C	Length of collector assembly	115 m
Freeze protection temperature	150°C	Number of modules per assembly	8
Min and max single flowrates	1 and 12 kg/s	Average surface-to-focus path length	2.15 m
Design min header flow velocity	2 m/s	Piping distance between assemblies	1 m
Design max header flow velocity	3 m/s	Absorber tube inner and outer diameters	0.076 and 0.08 m
Stow and deploy angles	170 and 10°	Glass envelope inner and outer diameters	0.115 and 0.12
		Design min and max header flow velocities	2 and 3 m/s

2.2 Modelling and Simulating Solar-Driven Pyrolysis, Thermolysis and Electrolysis Processes of H_2 Generation Coupled with Thermal Energy Storage (TES) and Rankine Cycle.

Modelling of these integrated H_2 generation systems was conducted in Aspen Plus with the application of Peng-Robinson and Non-Random Two-Liquid (NRTL) equation of states. Peng-Robinson equation of state allows the prediction of thermodynamic properties of some streams, while the involvement of NRTL equation of state was due to the presence of charged species. To accommodate moderate and minimal pressure deviation, the Ideal gas property is used. Mixed, conventional inert (CI) and non-conventional (NC) solids are substreams of the system. Both integrated H_2 generation technologies do follow the below assumptions.

- All processes are in steady state condition.
- Heat and pressure losses are neglected.
- Feeds operating temperature and pressure are ambient and atmospheric.
- Reformer and combustor input variables are taken from literature and result of parametric sensitivity analysis.
- Heat exchanger for biomass and H_2O decomposer.
- Absence of tar in the biomass decomposer because of the involvement of H_2O as a reaction media.
- Decomposition and volatilisation of biomass in the second phase and cracking in the last phase.
- 10 and 1 bar pressures for fluidised bed reactor (FBR) and electrolyte stack cell.
- Sulphur content in CH_4 gas is approximately 5% [35].
- Metal catalysts (Ni-based) undergone a regeneration process.
- Use of heater blocks for storage of hot and cold molten salt.
- Molten salt composed of 50wt% $NaNO_3$ and 50wt% KNO_3
- SO_2 for alkaline electrolysis of H_2O.
- Splitter for molten salt flowrate control.
- Absence of deactivation during multiple desorption-reduction cycles.

A detailed process simulation of integrated methane and biomass pyrolysis (IMBP) coupled with thermal energy storage (TED) and a steam cycle is shown in Fig. 4. The hybrid system consists of heat exchangers (HX), reactors, separators, mixers, splitters and hierarchy blocks. $CH-1$ to $CH-3$, and CH_4-F represent CH_4 flow streams. While H_2O-1 to H_2O-10 describe the flow of H_2O and steam. Hot-SA, M-SALT, SALT-F and Re-SALT represent a flow of molten salt. In the simulated model, the feed (CH_4) under ambient and atmospheric conditions exchanges heat with hot CH_4 from the high-temperature furnace to 350°C prior entering the desulphurisation zone where portion of H_2 was used to absorb the sulphur. CH_4 gas leaving the desulphurisation unit flows into the furnace to raise the temperature to 958°C and dropped to 703°C at the exit of HX-1. The hot feed (pure CH_4) enters the fluidised bed reactor (FBR) where CH_4 cracking in the presence of a Ni-based catalyst occurred. Cyclone and separator blocks separate solid from gas and H_2 from other end products. Unreacted CH_4 from the gas separator mix with CH_4 in the fifth mixer. While by$-CO_2$ product is captured by the exothermic reaction of CaO to produce $CaC0_3$. Heat recovered from FBR through the application of heat exchangers was utilised for heating the molten salt, biomass decomposition and pyrolysis. The first splitter controls the flowrate of hot molten salt at a fraction of 0.3/hour. While cold molten salt from the cold storage furnace is part of the feed after the first complete cycle of the integrated system. A fraction of 0.3/hour of hot molten salt is then used to transform H_2O into steam for a Rankine cycle with turbine intake and discharge pressure of 41 and 1 bar. Logarithmic mesh particle size distribution (PSD) with the upper and lower limit of 1 – 35 microns (μm) was considered during the process modelling. The fluidised bed reactor catalyst is Ni-based and exposed to a reaction temperature and pressure of 700°C and 10 bar to limit the amount of carbon deposition. Thermal energy needed for endothermic cracking of both CH_4 and biomass feedstocks is provided by the CSP system, and the heater block is assumed to be the CSP furnace in Aspen plus environment for adjustment of both activation energy and reaction temperature.

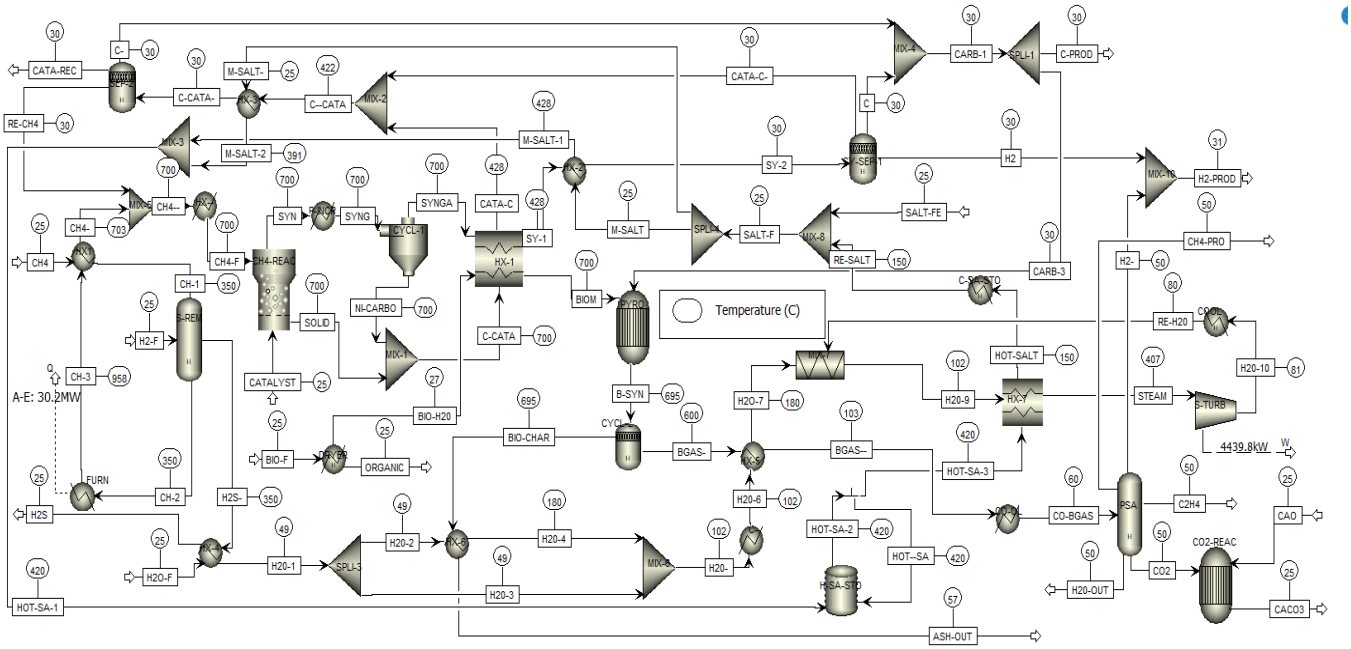

Figure 4: ASPEN Plus flow diagram for catalytic pyrolysis of CH_4 and biomass (CPMB).

To make use of thermal energy from the CSP system, the Aspen model of CH_4 and biomass pyrolysis coupled with TES and steam cycle was then transformed into a flow-driven dynamic Aspen model and called from the Simulink. The result of the simulated CSP system saved in the MATLAB workspace such as exit HTF intake and exit temperatures are used as input parameters to the Simulink model. In the Simulink environment, HTF intake and exit temperatures were connected to CH_4 and biomass pyrolysis furnace. Produced H_2 gas is assumed to be used to generate the heat required to raise the temperature of the CH_4 gas entering the sulphur removal unit to 350°C during the system start-up (first cycle). While another portion of H_2 by-product replaces fossil fuel backup during the initialisation of the CSP system. Process flowchart and flow diagram of the CSP-Aspen model of CH_4 and biomass pyrolysis coupled with TES and steam cycle are displayed in Fig. 5 and 6 with CH_4 gas as the working fluid.

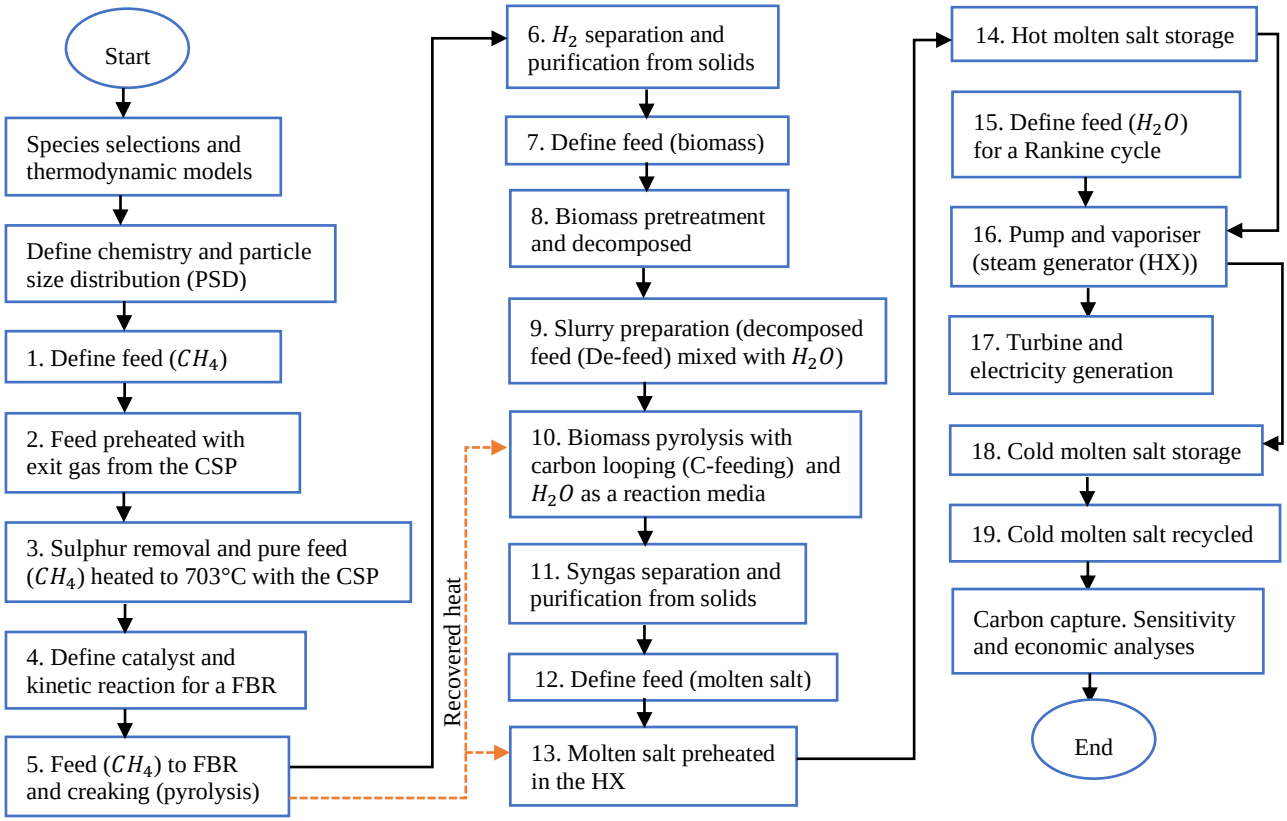

Figure 5: CSP-ASPEN flowchart for catalytic pyrolysis of methane (CH_4) and biomass (CPMB)

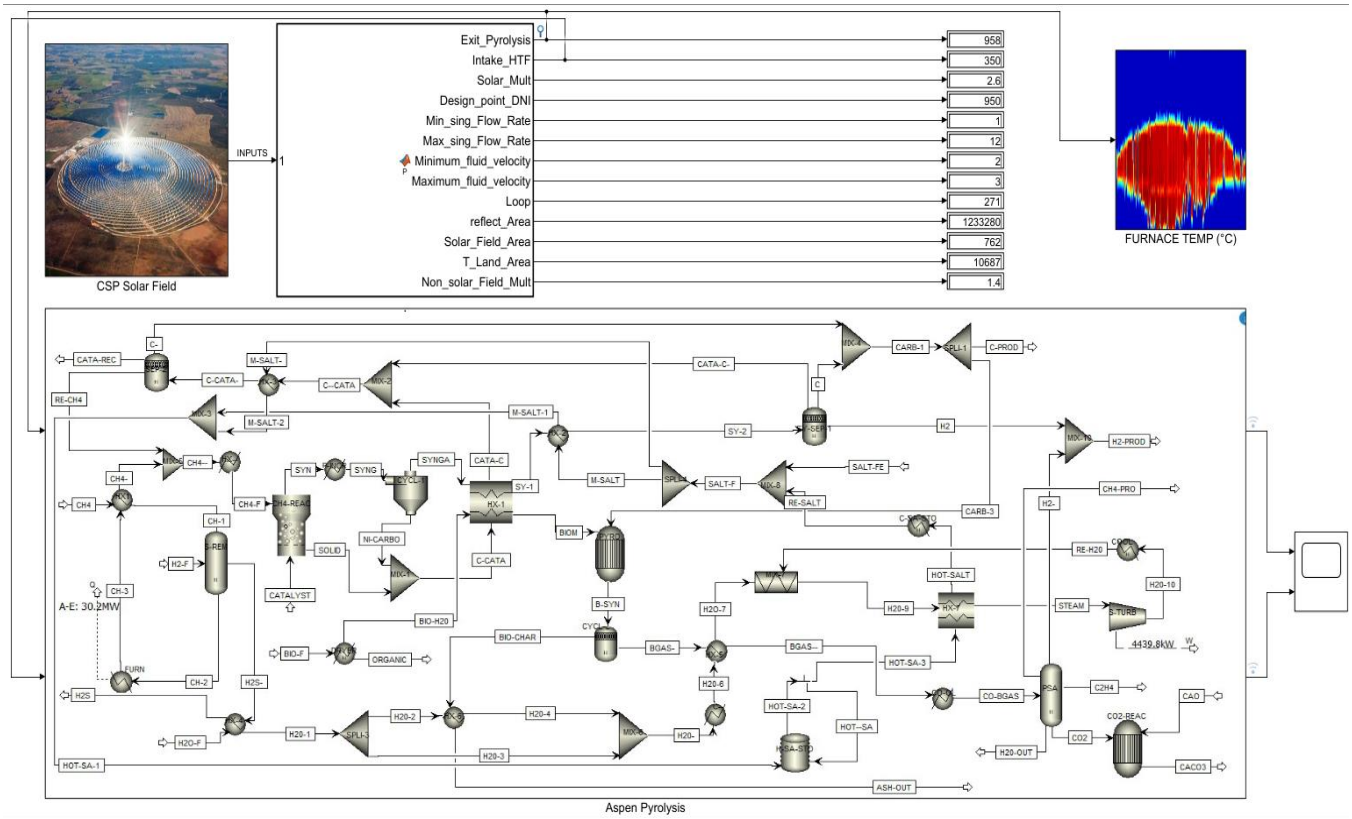

Figure 6: CSP-ASPEN Plus flow for catalytic pyrolysis of methane (CH_4) and biomass (CPMB).

The working principle of the CSP-Pyrolysis of methane and electrolysis of water (PMEW) coupled with TES and Rankine cycle is very similar to the CSP-CPMB (catalytic pyrolysis of methane and biomass) except for thermolysis of H_2SO_4 and electrochemical reaction to generate H_2 and O_2. The integrated technology consists of heat exchangers (HX), reactors for CH_4 pyrolysis, separators, mixers, splitters, electrolyte stacks and hierarchy blocks. The representation of CH_4, H_2O and molten salt flow streams are the same as that of the CPMB system. As the alkaline electrolyser cell (AEC) requires distilled H_2O to generate H_2, part of the exit heat from the sulphuric acid (H_2SO_4) reactor is used to achieve that through the application of HX. Thus, allowing H_2O to pass through HX-7 prior entering the AEC stack. Thermolysis of H_2SO_4 to generate sulphur dioxide (SO_2) prior entering the stack was also achieved by the recycling of wasted heat from FBR. Thermolysis of H_2SO_4 generated O_2 as one of the valuable by-products. While H_2 gas and regenerated H_2SO_4 from the AEC stack after the electrochemical reaction was separated and H_2SO_4 flows back to the thermolysis reactor as described in Eq 11. Recovered heat from thermal decomposition of H_2SO_4 is then used to generate supercritical steam for electrochemical splitting of H_2O through the application of SOEC. The supercritical steam enters the SOEC stack where electrolysis of H_2O as described in Eqs 6 – 8 occurs to generate both H_2 and O_2. H_2 generated from CH_4 pyrolysis and electrolysis of H_2O combined and stored. The process of incorporating the CSP system to provide the required thermal energy for CH_4 decomposition and thermolysis of H_2SO_4 as shown in Fig. 8 is the same as the integrated system displayed in Fig. 6. Process flowchart of the CSP-Aspen model of CH_4 pyrolysis and electrolysis of H_2O coupled with TES and steam cycle is displayed in Fig. 7.

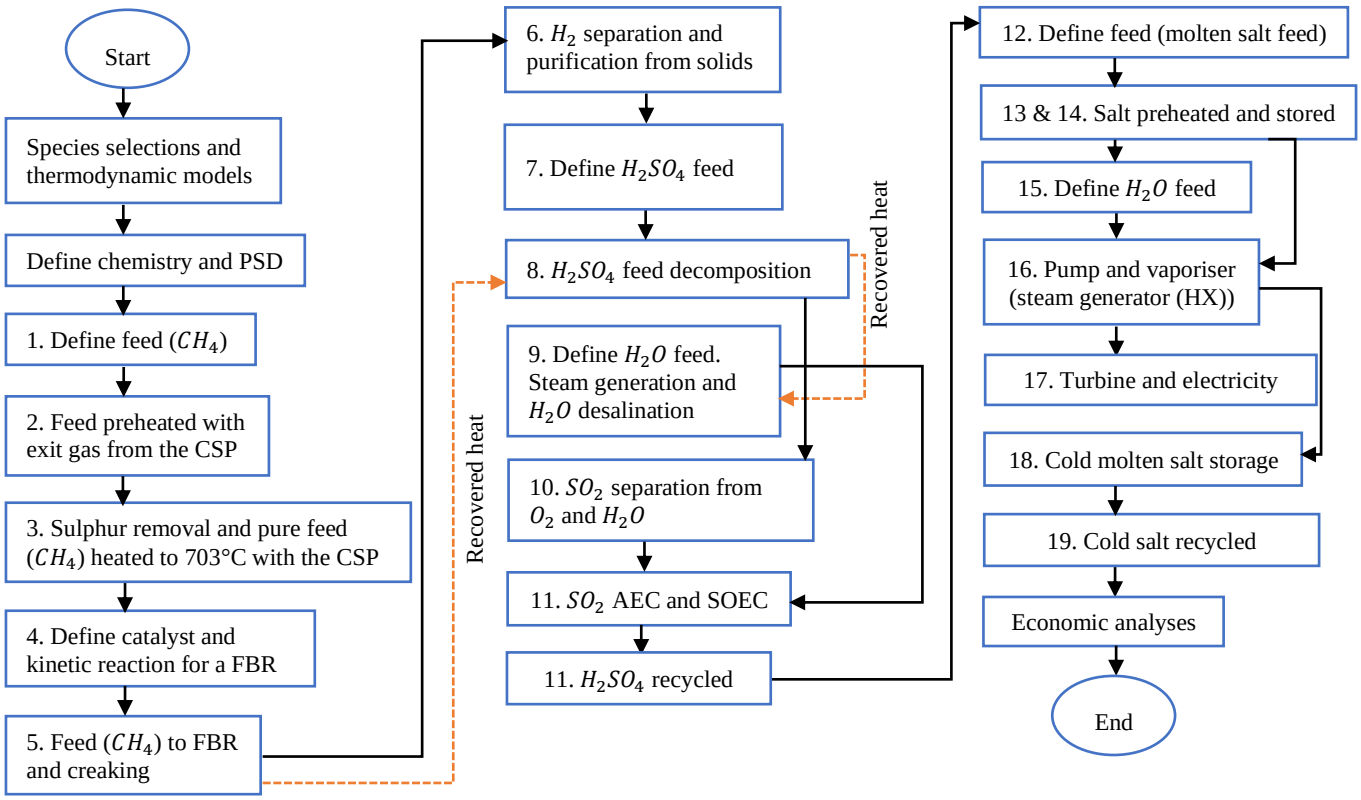

Figure 7: CSP-ASPEN flowchart for catalytic methane (CH_4) pyrolysis and H_2O electrolysis (CMPWE)

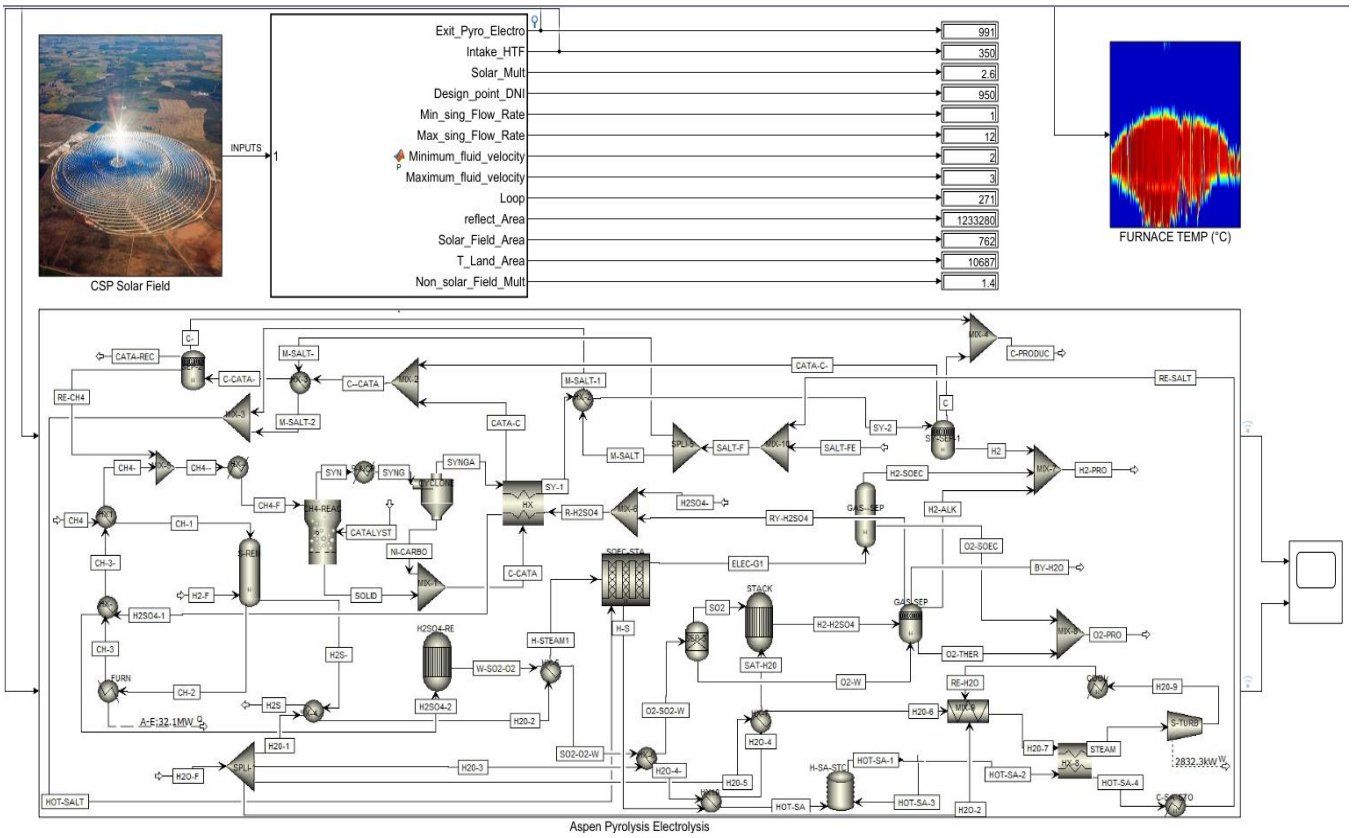

Figure 8: CSP-ASPEN Plus flow diagram for catalytic methane (CH_4) pyrolysis and H_2O electrolysis (CMPWE)

As mentioned by *Msheik, et al.* [7], noncatalytic CH_4 pyrolysis with an application of solar energy is needed to mitigate a drawback related to coking on the catalyst active site of catalytic CH_4 pyrolysis. Thus, a noncatalytic pyrolysis of CH_4 and H_2O electrolysis coupled with TES and Rankine cycle is modelled and simulated with the reactor operating temperature and pressure of 952°C and 1 bar. The operational principle is the same as CMPWE coupled with TES and Rankine cycle except for the

absence of Ni-based catalyst, the use of a different reactor for CH_4 cracking and recycling of H_2S. The modified system uses a conventional reactor and part of reactor exit heat to raise the feed (CH_4) temperature to 350°C prior entering the desulphurisation zone. The Aspen process flow diagram for a noncatalytic CH_4 pyrolysis and electrolysis of H_2O is depicted in Fig. 9.

Not long ago, Sorption Enhanced–Chemical Looping (SE-CL) which involves oxidation and reduction of oxygen carriers to produce syngas has been viewed as a promising option for CO_2 reuse and recycling. SE-CL include a reaction of hydrocarbon with oxygen carrier species and another reaction of CO_2 with solid specie like Nickel (Ni) to produce synthetic gas [36]. While the last step of SE-CL is a capture of unreacted by-CO_2. This work further investigate SE-CL using Ni-based oxygen carrier as an effort to recycle by-CO_2 and increase H_2 concentration as represented in Eqs 14 - 16. Fig. 10 displays the process simulation described in Equation 14 - 16 for reuse of both CH_4 and by-CO_2 by-products from biomass pyrolysis to generate more syngas before CO_2 capture.

$$CH_4 + NiO \leftrightarrow CO + 2H_2 + Ni \; \Delta H^0_{298} = 203kJ/mol \tag{14}$$

$$C0_2 + Ni \leftrightarrow NiO + CO \; \Delta H^0_{298} = 43kJ/mol \tag{15}$$

$$CaO + C0_2 \leftrightarrow CaC0_3 \; \Delta H^0_{298} = -179.8kJ/mol \tag{16}$$

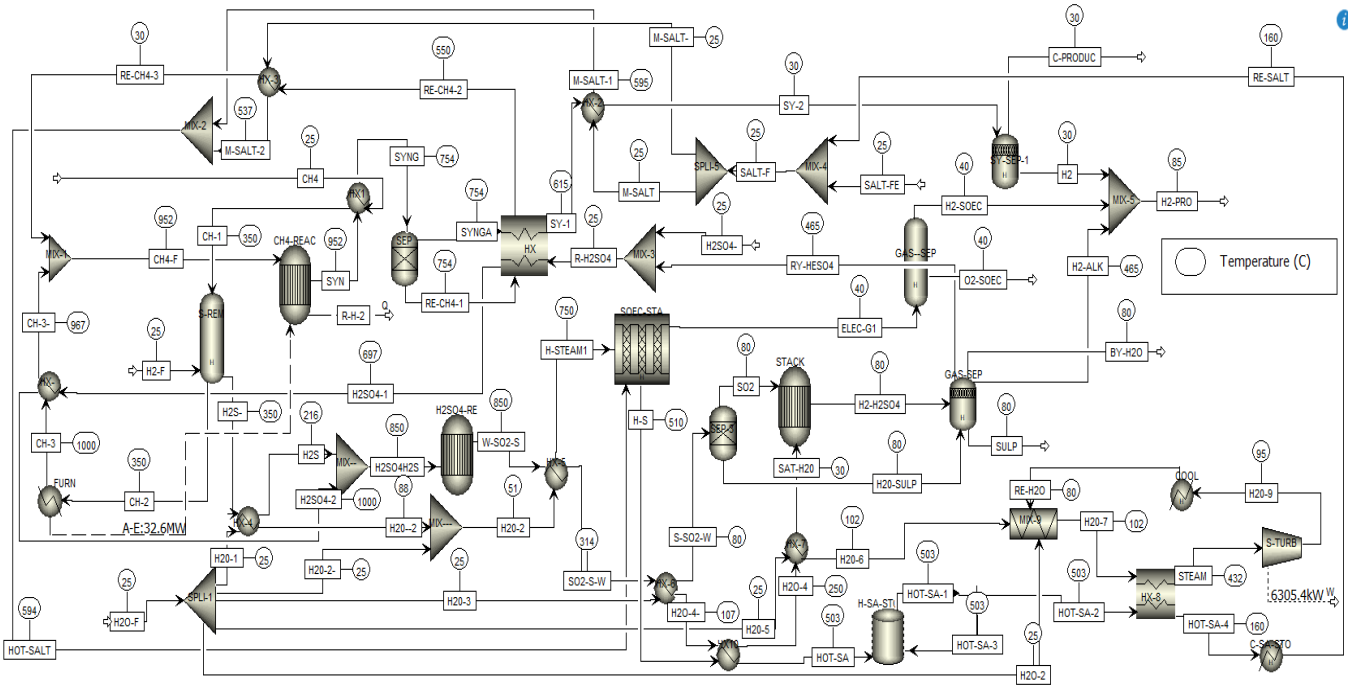
RE-CH4-3
RE-CH4-2
M-SALT-1
M-SALT-2
M-SALT
SYNG
CH4
SYNGA
SYN
CH4-REAC
CH4-F
CH-1
R-H2SO4
RE-CH4-1
H2SO4-
SALT-F
SALT-FE
RY-HESO4
H2-SOEC
O2-SOEC
H2
H2-PRO
H2-ALK
C-PRODUC
RE-SALT
Temperature (C)
H-STEAM1
SOEC-STA
ELEC-G1
BY-H2O
STACK
SO2
H2-H2SO4
SAT-H20
H20-SULP
SULP
H2S
H2SO4H2S
H2SO4-RE
W-SO2-S
H2SO4-1
H2SO4-2
H20-2
H20-1
H20-F
H2-F
H2S-
CH-3
CH-2
FURN
A-E:32.6MW
S-SO2-W
SO2-S-W
H20-4
H20-5
H20-6
H20-7
H20-8
H20-9
RE-H2O
COOL
S-TURB
STEAM
6305.4kW
HOT-SA-1
HOT-SA-2
HOT-SA-3
HOT-SA-4
HOT-SA
HOT-SALT
H-SA-STI
H-S
SEP-2
SEP-3
SEP-4
SEP-5
MIX-1
MIX-2
MIX-3
MIX-4
MIX-5
MIX-9
HX-1
HX-2
HX-3
HX-4
HX-5
HX-8
HX-9
SPLI-1
SPLI-5
SY-1
SY-2
ST-SEP-1
GAS-SEP
R-REF
R-H-2
CH-3-
CH-1
CH4-F
M-SALT-
H2-SOEC
H2-ALK
H2-PRO
BY-H2O
O2-SOEC
ELEC-G1
RE-H2O
H20-9
H20-7
H20-6
H20-5
H20-4
H20-2
H20-1
H20-F
H2-F
H2S-
CH-3
CH-2
H20-3
H20-2
H20-4-
H20-5
H20-6
H20-7
H20-8
H20-9
SO2-S-W
S-SO2-W
W-SO2-S
H2SO4-1
H2SO4-2
H2SO4-RE
H2SO4H2S
SAT-H20
H20-SULP
SULP
H-S
H-STEAM1
SOEC-STA
STACK
SO2
H2-H2SO4
GAS-SEP

3.0 Results and Discussions

The simulated result of the concentrating solar power (CSP) shows that increasing the outlet loop heat transfer fluid (HTF) decreases the flowrate of the working fluid. While maintaining the same flowrate of the CSP system with optimum operating temperature requires an increase in solar multiple which increases overall investment cost. Thus, incorporating MATLAB software into the SAM model made it possible for the simulation of the CSP system with exit HTF >800°C. The outcome of the simulated CSP result indicated that downsizing of the furnace and modification of the current systems are needed to maintain the aforementioned exit loop HTF temperature. By allowing 129.35$kmol/hr\ H_2$ flowrate which is 5% of 2579.5$kmol/hr\ CH_4$ gas present in the sulphur absorber, 99.99% of H_2S removal was recorded. This was crucial to minimise sulphur deposition on the Ni/dolomite catalyst present in the FBR despite Ni/dolomite catalyst resistance to sulphur deposition on its active site. About $7.7x10^{-8}kg/hr$ of sulphur content was estimated to be present in the CH_4 gas entering the FBR. Table 3 reports the feed, product, energy input (EI), power output (PO) and amount of carbon emission (CO_2e) of the simulated models. From the result Table, it can be seen that H_2 yield from integrated pyrolysis of CH_4 and biomass is lower in comparison with hybrid CH_4 pyrolysis and electrolysis of both alkaline and solid oxide. However, other valuable by-products like synthetic CH_4 gas was also produced. This was possible by the use of biomass feed with less ash content and both H_2O and carbon as reaction media to promote the rate of syngas formation at moderate operating temperatures. It can be observed that a small fraction of O_2 was present from the biomass pyrolysis by-products because of the formation of CO_2. Feeding part of produced carbon from CH_4 pyrolysis promoted fast biomass decomposition and full conversion of O_2 to CO_2 without the need for a catalyst in the reactor. Catalytic CH_4 pyrolysis and electrolysis of both alkaline and solid oxide show that carbon emissions can be prevented by the use of solar energy through the CSP plant to provide the required thermal energy for the endothermic decomposition of CH_4 feed. Thus, making the system more eco-friendly than integrated pyrolysis of CH_4 and biomass. However, integrated catalytic pyrolysis of CH_4 and biomass plant with a CSP system indicates that the need for cell stacks and electricity for electrochemical splitting of substrates can be avoided making it more energy efficient. Although, noncatalytic CH_4 pyrolysis and electrolysis of H_2O with recycled H_2S achieved lower H_2 concentration and higher H_2O formation with absence of O_2 by-product at the exit of H_2SO_4 reactor. As the reaction of H_2SO_4 with H_2S decrease syngas formation, the need for recycling H_2S in any of the integrated systems is unnecessary to maximise their efficiencies. Polygeneration pyrolysis of CH_4 and the electrolysis of H_2O process of extracting H_2 from other elements means that catalyst deactivation because of coking without efficiency drop is feasible by the use of a CSP system with an exit HTF of 1000°C; use of molten salt for syngas cooling to generate the required electricity for electrically power devices like pumps. Just like the current CSP system that uses molten salt as the working fluid and electricity generation in a Rankine cycle, both simulated technologies can generate more electricity during peak periods and at night with the use of CH_4 gas as the CSP working fluid. The introduction of thermal energy storage (TES) into both systems also shows that electricity production for up to 200 minutes during the shutdown of the CSP system and without an increase of H_2O flow volume is possible just like in existing CSP plants. This was possible by allowing an exit flowrate of 25 – 30% of molten salt from the TES tank per hour. Thermolysis of H_2SO_4 and electrolysis of H_2O with anodic oxidation of SO_2 shows higher H_2 yield and lower stack activation energy compared with SOEC. Thus, making the electrolysis system efficient enough for commercialisation. Due to the high greenhouse emissions associated with coal plants, an increase in the application of integrated CH_4 and biomass pyrolysis systems can eliminate the need for coal cracking for carbon production as one of the feedstocks for steel and cement production. Furthermore, pyrolysis of both CH_4 and biomass can reduce H_2 selling price when carbon as one of the by-products is sold. The integration of the SE-CL system into the hybrid pyrolysis of CH_4 and biomass plant has shown that the reuse and capture of CO_2 by-product and regeneration of sorbent (NiO) for more H_2 yield are possible. Thus, making the simulated technologies a promising one to substitute existing ones for efficiency improvement and reduction of carbon footprints in H_2 generation plants.

Table 3: Feed, product, EI, PO and CO_2e results of solar-driven pyrolysis and electrolysis processes of H_2 generation.

Streams	CPMB		CMPWE		NCMPWE	
	Feed	Product	Feed	Product	Feed	Product
CH_4 $(kmol/hr)$ (kg/hr)	2579.5	260.2	2579.5		2579.5	
Catalyst $(kmol/hr)$ (kg/hr)	11	11	11	11	11	11
Biomass $(kmol/hr)$ (kg/hr)	1037 78078					
H_2SO_4 $(kmol/hr)$ (kg/hr)			339.9 33337.2	339.9 33337.2	339.9 33337.2	339.9 33337.2
H_2O $(kmol/hr)$ (kg/hr)	4698.3 84642		640 11529.8	339.9 6124	688.7 12407.1	299.3 5391.9
CaO $(kmol/hr)$	439.4					

(kg/hr)	24642.7					
H_2 $(kmol/hr)$ Total	129.3	Pyrolysis: 5172 Biomass: 179 5351	129.3	Pyrolysis: 5172 AEC: 340 SOEC: 300 5812	129.3	Pyrolysis: 5172 AEC: 190.3 SOEC: 308 5670.3
Carbon $(kmol/hr)$	517.2	2068.7		2586		2586
O_2 $(kmol/hr)$ Total		$1.54x10^{-20}$		Thermal: 170 SOEC: 150 320		Thermal: 0 SOEC: 154 154
H_2S $(kmol/hr)$ (kg/hr)		129.3 4406.8		129.3 4406.8		
Sulphur $(kmol/hr)$ (kg/hr)						108.95 3493.6
C_2H_4 (kg/hr)		0.2				
Molten S $(kmol/hr)$ (kg/hr)	787.3 14184.1	787.3 14184.1	1893 174822	1893 174822	2326 214810.3	2326 214810.3
$CaCO_3$ $(kmol/hr)$ (kg/hr)		442.1 44244.4				
Ash (kg/hr)		5414.5				

Energy input (EI), power output (PO) and amount of carbon emission	CPMB	CMPWE	NCMPWE
Activation energy for furnace (MW)	30.2	32.1	32.6
Electricity output of turbine (MW)	4.4	2.8	6.3
Total energy requirement (MW) before loss	25.8	29.3	55.04
Carbon dioxide equivalent (CO_2e) in kg/min)	Captured		

As the heat transfer coefficient of the CH_4 pyrolysis feedstock is different from downstream units like biomass pyrolysis, thermolysis of H_2SO_4 and H_2O electrolysis, the total thermal energies required to operate both integrated systems under actual ideal reaction conditions are given in Table 4. The data in Table 4 was calculated by Aspen plus to estimate the required thermal energy to operate both simulated systems under design conditions. Nonetheless, both integrated systems can still operate under non-actual reaction conditions. However, the syngas (H_2) concentration rate will decrease in a scenario where the operating temperatures fall below, or the operating pressures go above designed operating conditions because of the endothermicity of both systems.

Table 4: Required thermal energy because of specific losses of different operating units and reaction parameters.

Catalytic pyrolysis of CH_4 and biomass (CPMB) couple with Rankine cycle with furnace input thermal energy of 30.2MW.				Catalytic CH_4 pyrolysis, thermolysis of H_2SO_4 and H_2O electrolysis couple with Rankine cycle with furnace input thermal energy of 30.2MW.			
Units	Required thermal energy (MW)	Tem (°C)	Pressure (bar)	Units	Required thermal energy (MW)	Tem (°C)	Pressure (bar)
Biomass pyrolysis reactor	16.1	695	10	Thermolysis of H_2SO_4 reactor	17.5	850	3
Biomass dryer and decomposer	16.8	100 - 695	10	AEC stack	13.3	80	1
Heat exchanges (HE)	28.6			SOEC stack	20.6	750	8
TES	0.01	420	10	Heat exchanges (HE)	54.6		
Total Energy Loss/required	61.51			Total Energy required	106		
Total thermal energy required	87.31 (61.51+ 25.8)			Total thermal energy required	135.3 (106+29.3)		

Kinetic and fluidised bed reactor (FBR) governing pyrolysis of methane (CH_4)

The power law kinetic reaction for CH_4 cracking to generate H_2 and carbon as end products were based on the Arrhenius equation expressed in Eq 14.

$$kT = Ae^{-\frac{E_A}{RT}} \quad (14)$$

Where $k(T), E, A, T, and\ R$ represent temperature function, activation energy (kJ/mol), pre-exponential factor per min, the absolute temperature in Kelvin, and universal gas constant ($8.314\ J/mol/K$). While the specific fluidised bed mass is dictated by hydrodynamics reaction kinetics. Although, a bed mass of 6087kg was utilised. The activation energy for any given reaction is influenced by the type of catalyst used during the decomposition phase. For instance, *Ashik, et al.* [37] mentioned that between $50 - 90\ kJ/mol$ are activation energy for both Ni-based and carbon catalysts respectively. While *Geng, et al.* [5] assumed that the initial thermal decomposition of CH_4 gas over an Fe_2O_3 catalyst to generate H_2 can be represented as

$$r_{CH_4,O} = Ae^{-\frac{E_A}{RT}} * P_{CH_4}^{2.27} = 10605.2e^{-\frac{60266}{T}} * P_{CH_4}^{2.27} \quad (15)$$

$K = 80734, n = 0$ and $E = 5100kJ/mol$ were kinetic parameters utilised for each of the simulated plants. The unit of the fluidised bed reactor (FBR) is made up of solid and liquid phases. Thus, utilising 0.1m/sec specific velocity and 3 decay constant of Elutriation model; 6000 and 0.02m orifices number and diameter, while keeping the particle size distribution (PSD). The height and constant diameter of the discharge phase of the FBR were kept at 4 and 5 with 0 for the solid discharge location for adequate disengagement of the catalyst. Keeping FBR solid discharge location at zero (0) allows a small fraction of catalyst and carbon discharge at a solid weir. 10 bar operating pressure was kept for FBR due to the minimal pressure impact on the reactor, eliminating the need for pressure optimisation and minimising coke formation.

Temperature and pressure effect on methane (CH_4) decomposition.

The need for the pressure effect on the catalyst is disregarded as it has been reported that any pressure increase accelerates the catalyst feed rate by reducing solid hold-up [6]. In this work, parametric sensitivity analyses were performed to study the effects of temperature and pressure in noncatalytic CH_4 pyrolysis reactors on product formation and purity as displayed in Fig. 11 and 12. Reaction pressure and temperature between 1-30 bars and from 400-1500°C were utilised during the analyses for variation study of syngas composition. It found that an increase in reaction temperature increases the rate of syngas concentration. In contrast, pressure increase decreases syngas formation which opposes temperature increase. The result of these analyses indicates that syngas composition and concentration under endothermic reaction conditions are favourable to high reaction temperature and low pressure [38]. Both operating reaction parameters of a noncatalytic methane decomposition reactor (temperature and pressure) were kept at 952°C and 10 bars by taking the advantage of recycling unreacted feedstock. The result of noncatalytic CH_4 pyrolysis operating at the aforesaid temperature and pressure shows less than 5% syngas concentration without undecomposed feedstock recycling. Thus, re-entering unreacted CH_4 feed from the separator unit to the noncatalytic reactor achieved nearly the same syngas formation with higher activation energy in comparison with catalytic methane decomposition. As the feed is just CH_4, the study of carbon ratio was neglected. Nonetheless, the use of equilibrium reactors eliminates the need for the study of steam to carbon ratio (S/C) of biomass pyrolysis.

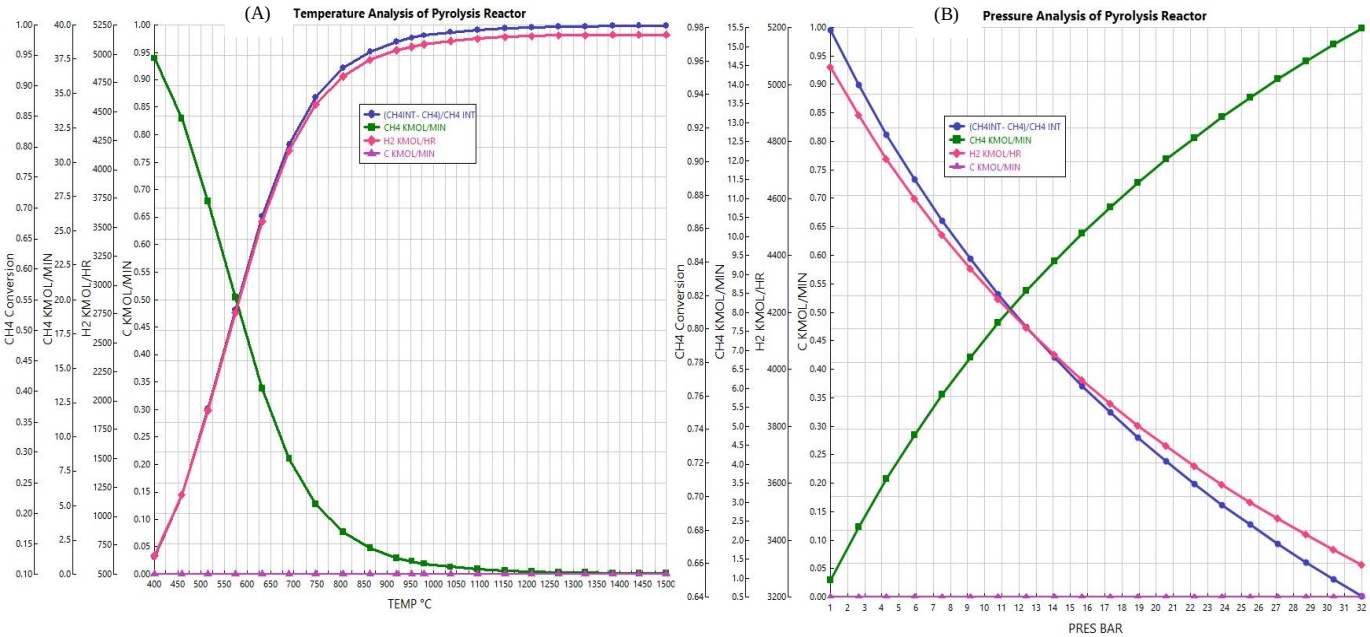

Figure 11: (A) Temperature and (B) pressure effects on CH_4 conversion to H_2 and Carbon.

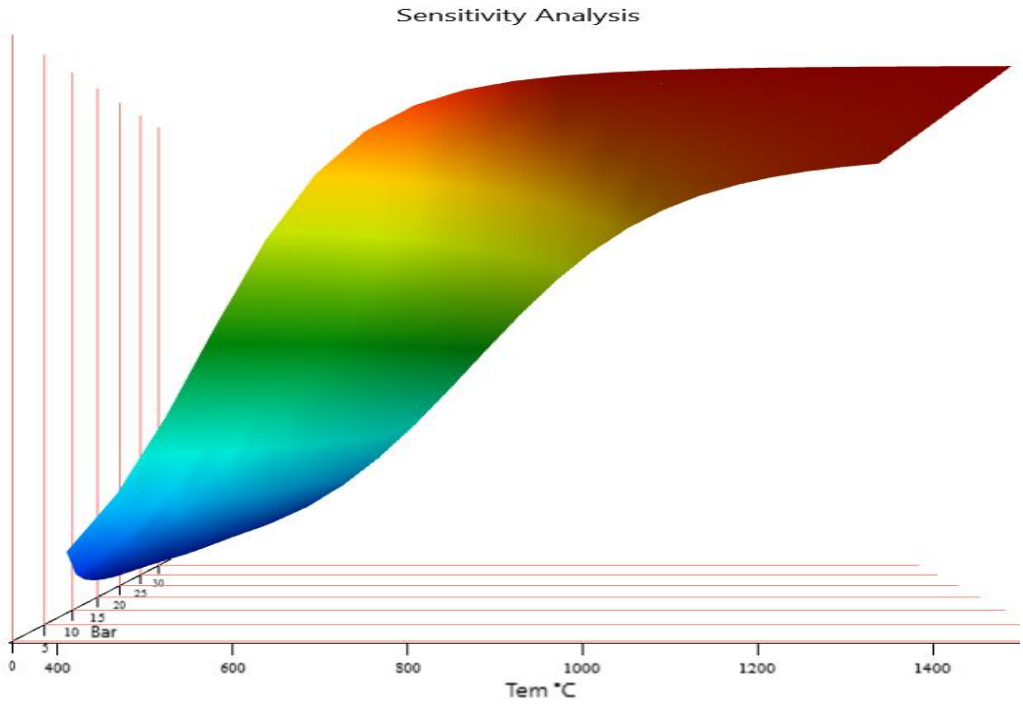

Figure 12: Temperature and pressure effects on CH_4 conversion to H_2 and Carbon.

Model validation and comparison

Tables 4 represent model validation with published data. The validated model was carried out on CH_4 pyrolysis, biomass pyrolysis and electrolysis of H_2O. Validated biomass pyrolysis and electrolysis of H_2O have different intake flowrates because both downstream subsystems are dependent on the amount of recovered thermal energy from CH_4 pyrolysis reactor. It can be seen from the validation Table that the present study agrees with the published data with marginal differences. In addition, it can be observed that both simulated hybrid models have the capacity to achieve carbon neutrality upon the modification and upgrading of the existing CSP plants to accommodate CH_4 as the working fluid with an exit HTF temperature up to 1000°C.

Table 5: Model validation

CH_4 pyrolysis			Biomass pyrolysis		
Operating parameters	This work	Riley, et al. [6]	Operating parameters	This work	[39]
CH_4 Feed flowrate $(kmol/hr)$	2579.5	2586	Biomass feed rate	78078 kg/hr	10 - 100 kg/hr
Catalyst feed flowrate (kg/hr)	11	11	H_2O feed rate	84642 kg/hr	
Pyrolysis operating temperature	700°C	700°C	Biomass operating temperature	695°C	350 - 750°C
Reformer operating pressure	10 bar	9.2 – 10 bar	Biomass operating pressure	10 bar	1 – 10 bar
H_2 yield $(kmol/hr)$	5172	5173	H_2 yield (wt.%)	>8	6.86
Carbon yield $(kmol/hr)$	2586	2587	Carbon yield (wt.%)		47.67
H_2 to carbon ratio	2:1	2:1			

Biomass pyrolysis extended			H_2O electrolysis	This work (AEC with H_2SO_4)	This work (SOEC)	SOE [40]	PEM [41]	AEL [41]
Feedstock	Temperature °C	H_2 yield (wt.%)	H_2O flowrate (kg/hr)	12248	5404.6	110,326	109,435	108,443
Hemicellulose	900	8.8 [42]	H_2 yield (kg/hr)	685.3	5404.6	12,122	12,122	12,122
Cellulose	900	5.5 [42]	O_2 yield (kg/hr)	5438.7	4799.8	96,213	97,179	96,212

Lignin	900	20.8 [42]	Activation energy (MW)	30.8 (17.5 + 13.3)	20.6	416	642	590
Sludge from the biogas plant	500	11.6 [43]						
Cow manure	550	25 [44]						
Oat straw	600	10 [45]						

Economic analysis

Unlike one of the cheapest and most used technology (steam methane reforming (SMR)) for H_2 production which generates 11.5 tonnes of CO_2 for every tonne of H_2, this integrated system captures CO_2 by-product and utilises CSP as an energy source [46]. The simulated model result shows that pyrolysis of CH_4 requires less thermal energy and more CH_4 feed due to the absence of shift reactions compared to SMR. As reported by *Parkinson, et al.* [46], for 200kta of H_2 output by SMR at 80% conversion efficiency, a total of 500kta of CH_4 is consumed and $219M per year is estimated to be a total production cost (TPC) at $1.10/kg of H_2 selling price. In contrast, CH_4 pyrolysis requires an additional 300kta of CH_4 feedstock and costs $64.4M for TPC because of the removal of downstream units. Between $1.18/kg to $1.89/kg is reported as H_2 selling price of CH_4 pyrolysis [46]. While 77% TPC of CH_4 pyrolysis was attributed to utility with the use of an electric arc heater (EAH) for endothermic cracking of the CH_4 feed. Nevertheless, the fixed capital investment of CH_4 pyrolysis operating with EAH is estimated to reach $643M with a land factor of 10. While an additional 129M is required to cover working capital and start-up cost [46]. Due to the decrease in capital cost of CSP systems, replacing EAH with CSP with TES unit can reduce H_2 selling price of CH_4 pyrolysis. For example, it was mentioned that as of 2020, CSP systems will experience a capital cost reduction between 28% to 40% because of an increase in competitive supply chains [47]. In addition, an increase in CSP installation capacity and choosing a location with high solar direct normal irradiance (DNI) will further reduce the Levelised cost of electricity (LCOE) [47]. As reported by Wright, et al. [48], utilities cost around $9.1M for biomass fast pyrolysis with 2000Mta of H_2 output at 1.50/kg of H_2 selling price. H_2 selling price for both CH_4 and biomass pyrolysis are expected to decrease further as both plants can potentially replace coal plants to produce carbon by-products. At the moment, the Global carbon market (carbon black and graphitic) is growing, and carbon selling price is expected to reach $10/kg [6]. While H_2O desalination (production of distilled H_2O) cost $0.084/kg H_2 at $3.89/kg of H_2 selling price. Nevertheless, it was reported that the electrolysis process of H_2 product from renewable pathways cost between $5.10/kg to 10.3/kg [49]. The high cost of H_2 production from renewable sources like electrolysis is expected to decrease with the transition to cheaper electrodes and membranes, and integration into other processes [50]. Currently, between $2.2/kg to $2.9/kg are H_2 selling price for SMR with a carbon capture and storage (CCS) system [6]. While the simulated system (CH_4 and biomass pyrolysis) can achieve H_2 selling price below $2.94/kg when other valuable by-products like carbon (C) and ethene (C_2H_4) are sold. In addition, more reduction of H_2 selling price of both integrated systems will be expected during the rainy season because of low ambient and module temperatures. For example, *Singh, et al*. [51] analysis of solar power variation in different seasons maintained that dust on solar panels/mirrors, low solar insolation and small solar window in summer and winter seasons decrease the efficiency of solar panels/mirrors despite high solar insolation in the summer period. Furthermore, CSP improvement by installing it in MENA (the Middle East and North Africa) regions that experience more sunshine during the day has also been suggested [30]. For instance, *Lilliestam & Pitz-Paal.* [52] reported $0.07/kWh cost of electricity from CSP systems operating in Dubai (DEWA IV) in contrast to $0.14/kWh in China [53] and concluded that further electricity cost reduction is expected. Therefore, efficiencies of both integrated systems of H_2 and other valuable by-products production are predicted to be higher during the rainy season regardless of the installed region. Table 6 compares existing and simulated H_2 production processes. While Table 7 illustrates Aspen economic and energy analysers.

Table 6: Comparison of current and simulated hydrogen production technologies.

Hydrogen production methods (H_2)	Advantages	Disadvantages	Cost ($/kg)	Efficiency (%)	References
SMR with CCS	Low cost and high efficiency.	High carbon emissions.	2.27-2.9	74-85	[13] [49]
Gasification	Low cost and high efficiency.	High carbon emissions.	1.91	35	[13] [49]
Pyrolysis	Cost less than SMR and minimal carbon footprints.	Catalyst deactivation and carbon emissions.	1.77-2.05	42.5	[13] [49]
Thermolysis	Chemical reuse within cycles and cost effective.	High carbon footprints because of high operating temperature.	2.31	52	[13] [49]

Electrolysis from renewable sources	High efficiency, carbon neutral and substrates availabilities.	Hight cost and energy intensive.	5.10-10.3	70	[13] [49]
Photocatalyst	Cost effective and less energy requirement.	Poor efficiency because of low substrate conversion and impurities.	9	0.06	[13] [49]
Photo-fermentation	Cost effective and less energy requirement.	Poor efficiency because of low substrate conversion and impurities.	2.83	0.1	[13] [49]
Dark fermentation	Cost effective and absence of light.	Poor efficiency because of low substrate conversion and impurities.	2.57	10.14	[54]
Simulated pyrolysis of CH_4 and biomass	Absence of carbon emission. Carbon capture. Use of renewable energy source. Production of other valuable by-products. Electricity generation through recovered heat. Cost effective and Good efficiency.	High energy requirement and coking.	1.7	35-50	This work
Simulated CH_4 pyrolysis and electrolysis of H_2O	Absence of carbon emission. Use of renewable energy source. Production of other valuable by-products. Chemical reuse within cycles. Electricity generation through recovered heat. Cost effective and Good efficiency.	High energy requirement and coking.	4.6-10.49	60-63	This work

Table 7: Aspen economic and energy analysers for (A) pyrolysis of CH_4 and biomass and (B) CH_4 pyrolysis and H_2O electrolysis

(A) Pyrolysis of CH_4 and biomass

Total Capital Cost [USD]	76,365,900
Total Operating Cost [USD/Year]	2,534,130
Total Raw Materials Cost [USD/Year]	0
Total Product Sales [USD/Year]	0
Total Utilities Cost [USD/Year]	696,219
Desired Rate of Return [Percent/'Year]	20
P.O. Period [Year]	0
Equipment Cost [USD]	24,770,700
Total Installed Cost [USD]	60,243,400

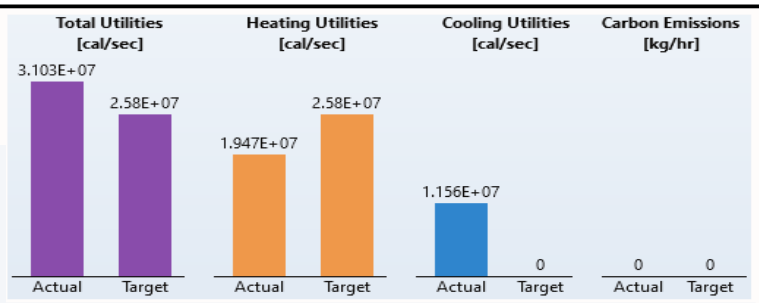

	Actual	Target	Available Savings	% of Actual
Total Utilities [cal/sec]	3.103E+07	2.58E+07	5.23E6	16.84
Heating Utilities [cal/sec]	1.947E+07	2.58E+07	-6330000.00	-32.54
Cooling Utilities [cal/sec]	1.156E+07	0	1.156E7	100.00
Carbon Emissions [kg/hr]	0	0	0.00	0.00

(B) CH_4 pyrolysis and H_2O electrolysis

Total Capital Cost [USD]	124,952,000
Total Operating Cost [USD/Year]	2,426,950
Total Raw Materials Cost [USD/Year]	0
Total Product Sales [USD/Year]	0
Total Utilities Cost [USD/Year]	315,913
Desired Rate of Return [Percent/'Year]	20
P.O. Period [Year]	0
Equipment Cost [USD]	39,077,000
Total Installed Cost [USD]	97,833,800

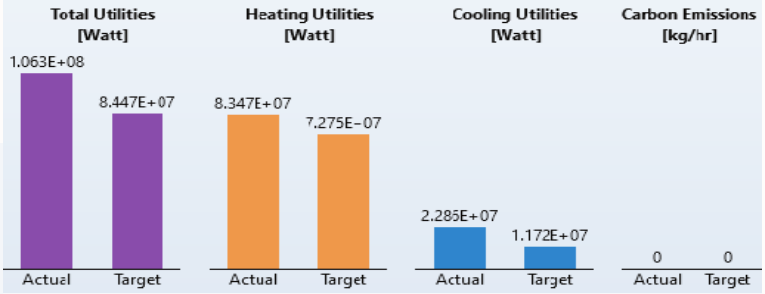

	Actual	Target	Available Savings	% of Actual
Total Utilities [Watt]	1.063E+08	8.447E+07	2.186E7	20.56
Heating Utilities [Watt]	8.347E+07	7.275E+07	1.072E7	12.85
Cooling Utilities [Watt]	2.286E+07	1.172E+07	1.114E7	48.73
Carbon Emissions [kg/hr]	0	0	0.00	0.00

Equivalent annual operating costs (EAOC) for each of the integrated systems are expected to exceed $3000M/year as [6] reported $188M/year EAOC from investigated work (methane pyrolysis) with feed and catalyst flowrates of 2586$kmol/hr$ and 11kg/hr. Furthermore, *Riley, et al.* [6] investigated work put H_2 selling price between 2.94/kg - $3.1/kg and concluded that between 60.7% - 66.6% of EAOC comes from CH_4 feedstock. With the estimated cost of $178/$m^2$ for parabolic trough collectors (PTC) CSP system reported in 2014 by *Kurup & Turchi*. [55], the total cost of the simulated plant (PT) is assumed to be $549M/year. Nonetheless, $329.4M/year is estimated to be the final cost of the simulated CSP (PT) system at a 40% cost reduction. While Aspen process economic analyser estimated $76.4M/year for pyrolysis of both CH_4 and biomass, and $125M/year for CH_4 pyrolysis and H_2O electrolysis. However, further cost reduction is expected when generated electricity through the Rankine cycle application substitute Aspen calculated cost of utilities. Between 5-6 years is estimated to be the desired rate of investment cost return. Therefore, simulated integrated plants not only can eliminate carbon emissions into the environment but can also reduce H_2 selling price in CH_4 and biomass pyrolysis, and electrolysis of H_2O. In a scenario where the operating temperature of the simulated innovative system furnace is unachievable in a modified existing CSP plant, a portion of produced H_2 can be burned to meet the desired operating temperature.

i) Use of CSP as a thermal energy source to eliminate the burning of fossil fuels in reactors' furnaces. ii) Application of thermal energy recovery to power downstream units such as thermolysis cracking of H_2SO_4 and steam generation for H_2O electrolysis of high and low temperatures. iii) Electricity generation through recovered thermal energy. iv) Enhancement of biomass decomposition through carbon looping and use of H_2O as a reaction media. v) Oxidation of SO_2 in the anode chamber of AEC to promote hydrogen evolution reaction are advantages of the simulated plants over current pyrolysis and electrolysis systems for H_2 production. In addition, TES application to generate high-temperature steam for H_2O electrolysis and a Rankine cycle; by-product CO_2 reuse for more H_2 production and by-product CO_2 capture are benefits of simulated plants over similar solar-driven pyrolysis. If followed up, this new approach will promote net-zero greenhouse emissions in integrated H_2 and electricity generation plants and substitute coal plants for carbon production.

Conclusion

Solar-driven pyrolysis and electrolysis processes have been reviewed, modelled and simulated as an alternative system to replace existing conventional ones for eco-friendly means of H_2 polygeneration methods. The result of noncatalytic pyrolysis of CH_4 showed that coking due to carbon deposition on the active site of the catalyst can be prevented with the use of a higher operating temperature. Nonetheless, catalytic pyrolysis of CH_4 with less coke formation is essential to reduce the activation energy required for feedstock decomposition. The simulated hybrid CH_4 and biomass pyrolysis achieved about a 10% reduction of H_2 selling price with the absence of carbon emission into the environment compared to the existing one. In addition, CH_4 and biomass pyrolysis has shown that it can substitute coal plants to produce carbon for steel and cement manufacturing. While CH_4 pyrolysis and H_2O electricity with anodic oxidation of SO_2 showed improvement in the hydrogen evolution reaction which increase the overall stack efficiency. Both simulated systems have illustrated that a portion of produced H_2 can substitute fossil fuels burning in a situation where the desired operating temperature of the CSP system is not being met. Between 5 - 6 years is estimated for return on investment for both simulated plants. The use of a non-polluting thermal energy source, the absence of carbon emission by capturing by-product CO_2, thermal energy storage for later use and electricity generation are advantages of both simulated systems.

CRediT authorship contribution statement

Linus Onwuemezie: Conceptualization, Methodology, Software, Validation, Formal analysis, Investigation, Writing – Original Draft. **Hamidreza Gohari Darabkhani:** Methodology, Software, Validation, Formal analysis, Investigation, Writing – Original Draft, Writing – Review & Editing, Supervision, Project administration **Mohammad Moghimi Ardekani:** Software, Validation, Formal analysis, Investigation, Writing – Original Draft, Writing – Review & Editing, Supervision.

Declaration of Competing Interest

The authors declare that they have no known competing financial interests or personal relationships that could have appeared to influence the work reported in this paper.

References

[1] IPCC, "Summary for Policymakers of IPCC Special Report on Global Warming of 1.5°C approved by governments," 2022. [Online]. Available: https://www.ipcc.ch/2018/10/08/summary-for-policymakers-of-ipcc-special-report-on-global-warming-of-1-5c-approved-by-governments/. [Accessed 21 09 2022].

[2] I. Staffell, D. Scamman, A. V. Abad, P. Balcombe, P. E. Dodds, P. Ekins, N. Shah and a. K. R. Ward, "The role of hydrogen and fuel cells in the global energy system," *Energy & Environmental Science,* no. 12, pp. 463-491, 2019.

[3] M. Z. Jecobson, "Atmosheric Pollution: History, Science, and Regulation," Cambridge University Press, Cambridge , 2002.

[4] M. Ni, M. K. H. Leung and a. D. Y. Leung, "Technological development of hydrogen production by solid oxide electrolyzer cell (SOEC)," *International Journal of Hydrogen Energy,* vol. 33, no. 9, pp. 2337 - 2354, 2008.

[5] S. Geng, Z. Han, Y. Hu, Y. Cui, J. Yue, J. Yu and a. G. Xu, "Methane Decomposition Kinetics over Fe_2O_3 Catalyst in Micro Fluidized Bed Reaction Analyzer," *Industrial & Engineering Chemistry Research,* vol. 57, p. 8413 − 8423, 2018.

[6] J. Riley, C. Atallah, R. Siriwardane and a. R. Stevens, "Technoeconomic analysis for hydrogen and carbon Co-Production via catalytic pyrolysis of methane," *International Journal of Hydrogen Energy,* pp. 1 - 21, 2021.

[7] M. Msheik, S. Rodat and a. S. Abanades, "Methane Cracking for Hydrogen Production: A Review of Catalytic and Molten Media Pyrolysis," *Energies,* vol. 14, p. 3107, 2021.

[8] A. Abánades, C. Rubbia and a. D. C. Salmieri, "Technological challenges for industrial development of hydrogen production based on methane cracking," *Energy,* vol. 46, no. 1, pp. 359 - 363, 2012.

[9] H. Qiu, J. Ran, X. Huang, Z. Ou and a. J. Niu, "Unrevealing the influence that preparation and reaction parameters have on Ni/Al_2O_3 catalysts for dry reforming of methane," *International Journal of Hydrogen Energy,* vol. 47, no. 80, pp. 34066 - 34074, 2022.

[10] S. Patel, S. Kundu, P. Halder, M. H. Marzbali, K. Chiang, A. Surapaneni and a. K. Shah, "Production of hydrogen by catalytic methane decomposition using biochar and activated char produced from biosolids pyrolysis," *International Journal of Hydrogen Energy,* vol. 45, no. 55, pp. 29978 - 29992, 2020.

[11] C. Guizani, M. Jeguirim, S. Valin, L. Limousy and a. S. Salvador, "Biomass Chars: The Effects of Pyrolysis Conditions on Their Morphology, Structure, Chemical Properties and Reactivity," *Energies,* vol. 10, p. 796, 2017.

[12] M. N. Uddin, W. W. Daud and a. H. F. Abbas, "Potential hydrogen and non-condensable gases production from biomass pyrolysis: Insights into the process variables," *Renewable and Sustainable Energy Reviews,* vol. 27, pp. 204 - 224, 2013.

[13] P. Nikolaidis and a. A. Poullikkas, "A comparative overview of hydrogen production processes," *Renewable and Sustainable Energy Reviews,* vol. 67, pp. 597 - 611, 2017.

[14] A. Li, H. Han, S. Hu, M. Zhu, Q. Ren, Y. Wang, J. Xu, L. Jiang, S. Su and a. J. Xiang, "A novel sludge pyrolysis and biomass gasification integrated method to enhance hydrogen-rich gas generation," *Energy Conversion and Management,* vol. 254, p. 115205, 2022.

[15] B. Luna-Murillo, M. Pala, A. L. Paioni, M. Baldus, F. Ronsse, W. Prins, P. C. A. Bruijnincx and a. B. M. Weckhuysen, "Catalytic Fast Pyrolysis of Biomass: Catalyst Characterization Reveals the Feed-Dependent Deactivation of a Technical ZSM-5-Based Catalyst," *ACS Sustainable Chemistry & Engineering,* vol. 9, no. 1, p. 291 – 304, 2020.

[16] C. R. Ellison and a. D. Boldor, "Mild upgrading of biomass pyrolysis vapors via ex-situ catalytic pyrolysis over an iron-montmorillonite catalyst," *Fuel,* vol. 291, p. 120226, 2021.

[17] M. A. Khan, H. Zhao, W. Zou, Z. Chen, W. Cao, J. Fang, J. Xu, L. Zhang and a. J. Zhang, "Recent Progresses in Electrocatalysts for Water Electrolysis," *Electrochemical Energy Reviews,* vol. 1, no. 4, pp. 483 - 530, 2018.

[18] X. Tang, L. Xiao, C. Yang, J. Lu and a. L. Zhuang, "Noble fabrication of NieMo cathode for alkaline water electrolysis and alkaline polymer electrolyte water electrolysis," *International Journal of Hydrogen Energy,* vol. 39, no. 7, pp. 3055 - 3060, 2014.

[19] M. Bodner, A. Hofer and a. V. Hacker, "H_2 generation from alkaline electrolyzer," *WIREs Energy and Environment,* vol. 4, no. 4, pp. 365 - 381, 2015.

[20] S. Díaz-Abad, M. Millán, M. A. Rodrigo and a. J. Lobato, "Review of Anodic Catalysts for SO_2 Depolarized Electrolysis for "Green Hydrogen" Production," *Catalysts ,* vol. 9, no. 1, p. 63, 2019.

[21] Q. Zhao, M. Hou, S. Jiang, J. Ai, L. Zheng and a. Z. Shao, "Excellent Sulfur Dioxide Electrooxidation Performance and Good Stability on a Fe-N-Doped Carbon-Cladding Catalyst in H_2SO_4," *The Electrochemical Society,* vol. 164, pp. 456 - 462, 2017.

[22] C. Tangkusonjit, T. Pinnarat and a. Y. Patcharavorachot, "Comparative study of hydrogen production from solid oxide electrolysis cell with different electrolyte types," Muang Pattaya, 2018.

[23] A. Nechache and a. S. Hody, "Alternative and innovative solid oxide electrolysis cell materials: A short review," *Renewable and Sustainable Energy Reviews,* vol. 149, p. 111322, 2021.

[24] X. Sun, P. V. Hendriksen, M. Mogensen and a. M. Chen, "Degradation in Solid Oxide Electrolysis Cells During Long Term Testing," *FuelCells,* vol. 19, no. 6, pp. 740 - 747, 2019.

[25] K. Im-orb, N. Visitdumrongkul, D. Saebea, Y. Patcharavorachot and a. A. Arpornwichanop, "Flowsheet-based model and exergy analysis of solid oxide electrolysis cells for clean hydrogen production," *Journal of Cleaner Production,* vol. 170, pp. 1 - 13, 2018.

[26] H. Nami, O. B. Rizvandi, C. Chatzichristodoulou, P. V. Hendriksen and a. H. L. Frandsen, "Techno-economic analysis of current and emerging electrolysis technologies for green hydrogen production," *Energy Conversion and Management,* vol. 269, p. 116162, 2022.

[27] S. Baykara, "Experimental solar water thermolysis," *International Journal of Hydrogen Energy,* vol. 29, no. 14, pp. 1459 - 1469, 2004.

[28] M. B. Gorensek, C. Corgnale, J. A. Staser and a. J. W. Weidner, "Solar Thermochemical Hydrogen (STCH) Processes," *The Electrochemical Society Interface,* vol. 27 , pp. 53 - 56, 2018.

[29] A. Boretti, J. Nayfeh and a. W. Al-Kouz, "Validation of SAM Modeling of Concentrated Solar Power Plants," *Energies ,* vol. 13, p. 1949, 2020.

[30] A. Azouzoute, A. A. Merrouni and a. S. Touili, "Overview of the integration of CSP as an alternative energy source in the MENA region," *Energy Strategy Reviews,* vol. 9, p. 100493, 2020.

[31] M. Labordena, A. Patt, M. D. Bazilian, M. Howells and a. J. Lilliestam, "Impact of political and economic barriers for concentrating solar power in Sub-Saharan Africa," *Energy Policy,* vol. 102, pp. 72 - 72, 2017.

[32] I. F. Elbaba and a. P. T. Williams, "Deactivation of Nickel Catalysts by Sulfur and Carbon for the Pyrolysis−Catalytic Gasification/Reforming of Waste Tires for Hydrogen Production," *Energy Fuels,* vol. 28, p. 2104 – 2113, 2014.

[33] Y. Kato, R. Enomoto, M. Akazawa and a. Y. Kojima, "Characterization of Japanese cedar bio-oil produced using a bench-scale auger pyrolyzer," *SpringerPlus,* vol. 5, p. 177, 2016.

[34] F. Popescu, R. Mahu, I. V. Ion and a. E. Rusu, "A Mathematical Model of Biomass Combustion Physical and Chemical Processes," *Energies,* vol. 13, p. 6232, 2020.

[35] A. E. Lutz, R. W. Bradshaw, L. Bromberg and a. A. Rabinovich, "Thermodynamic analysis of hydrogen production by partial oxidation reforming," *International Journal of Hydrogen Energy,* vol. 29, no. 8, pp. 809 - 816, 2004.

[36] M. R. a. P. Ramos, "H_2 production with CO_2 capture by sorption enhanced chemical-looping reforming using NiO as oxygen carrier and CaO as CO_2 sorbent," *Fuel Processing Technology,* vol. 96, pp. 27 - 36, 2012.

[37] U. Ashik, W. W. Daud and a. H. F. Abbas, "Methane decomposition kinetics and reaction rate over Ni/SiO_2 nanocatalyst produced through co-precipitation cum modified Stöber method," *International Journal of Hydrogen Energy,* vol. 42, no. 2, pp. 938 - 952, 2017.

[38] H. L. Chatelier, "On a general statement of the laws of chemical equilibria," Gauthier-Villars, Paris , 1884.

[39] A. Visconti, M. Miccio and a. D. Juchelková, "An Aspen Plus® tool for simulation of lignocellulosic biomass pyrolysis via equilibrium and ranking of the main process variables," *International Journal of Mathematical Models and Methods in Applied Sciences,* vol. 9, pp. 71 - 86, 2015.

[40] M. Yousaf, A. Mahmood, A. Elkamel, M. Rizwan and a. M. Zaman, "Techno-economic analysis of integrated hydrogen and methanol production process by CO_2 hydrogenation," *International Journal of Greenhouse Gas Control,* vol. 115, p. 103615, 2022.

[41] Y. Muazzam, M. Yousaf, M. Zaman, A. Elkamel, A. Mahmood, M. Rizwan and a. M. Adnan, "Thermo-Economic Analysis of Integrated Hydrogen, Methanol and Dimethyl Ether Production Using Water Electrolyzed Hydrogen," *Resources* , vol. 11, p. 85, 2022.

[42] H. Yang, R. Yan, H. Chen, D. H. Lee and a. C. Zheng, "Characteristics of hemicellulose, cellulose and lignin pyrolysis," *Fuel,* vol. 86, no. 12 - 13, pp. 1781 - 1788, 2007.

[43] F. Monlau, C. Sambusiti, N. Antoniou, A. Barakat and A. Zabaniotou, "A new concept for enhancing energy recovery from agricultural residues by coupling anaerobic digestion and pyrolysis process," *Applied Energy,* vol. 148, pp. 32 - 38, 2015.

[44] J. Karaeva, S. Timofeeva, A. Kovalev, D. Kovalev, M. Gilfanov, V. Grigoriev and a. Y. Litti, "CO-PYROLYSIS of agricultural waste and estimation of the applicability of pyrolysis in the integrated technology of biorenewable hydrogen production," *International Journal of Hydrogen Energy,* vol. 47, no. 23, pp. 11787 - 11798, 2022.

[45] A. Mlonka-Mędrala, P. Evangelopoulos, M. Sieradzka, M. Zajemska and a. A. Magdziarz, "Pyrolysis of agricultural waste biomass towards production of gas fuel and high-quality char: Experimental and numerical investigations," *Fuel,* vol. 296, p. 120611, 2021.

[46] B. Parkinson, J. W. Matthews, T. B. McConnaughy, D. C. Upham and a. E. W. McFarland, "Techno-Economic Analysis of Methane Pyrolysis in Molten Metals: Decarbonizing Natural Gas," *Chemical Engineering & Technology,* vol. 40, no. 6, pp. 1022 - 1030, 2017.

[47] IRENA, "Renewable energy technologies: cost analysis series," vol. 1, no. 2/5, p. 5, 2012.

[48] M. M. Wright, J. A. Satrio, R. C. Brown, D. E. Daugaard and a. D. D. Hsu, "Techno-Economic Analysis of Biomass Fast Pyrolysis to Transportation Fuels," NREL, Colorado, 2008.

[49] M. Younas, S. Shafique, A. Hafeez, F. Javed and a. F. Rehman, "An Overview of Hydrogen Production: Current Status, Potential, and Challenges," *Fuel,* vol. 316, p. 123317, 2022.

[50] T. Terlouw, C. Bauer, R. McKenna and a. M. Mazzotti, "Large-scale hydrogen production via water electrolysis: a techno-economic and environmental assessment," *Energy & Environmental Science,* vol. 15, pp. 3583 - 3602, 2022.

[51] V. P. Singh, V. Vijay, G. S. H.a, D. K. Chaturvedi and a. N. Rajkumar, "Analysis of solar power variability due to seasonal variation and its forecasting for Jodhpur region using Artificial Neural Network," *CPRI,* vol. 9, no. 3, pp. 140 - 148, 2013.

[52] J. Lilliestam and a. R. Pitz-Paal, "Concentrating solar power for less than USD 0.07 per kWh: finally the breakthrough," *Renewable Energy Focus,* vol. 26, pp. 17 - 21, 2018.

[53] Y. Xu, J. Pei, J. Yuan and a. G. Zhao, "Concentrated solar power: technology, economy analysis, and policy implications in China," *Environmental Science and Pollution Research,* vol. 29, p. 1324 – 1337, 2021.

[54] H.-Y. Ren, B.-F. Liu, F. Kong, L. Zhao, J. Ma and a. N.-Q. Ren, "Favorable energy conversion efficiency of coupling dark fermentation and microalgae production from food wastes," *Energy Conversion and Management,* vol. 166, pp. 156 - 162, 2018.

[55] P. Kurup and a. C. S. Turchi, "Parabolic Trough Collector Cost Update for the System Advisor Model (SAM)," NREL, Colorado, 2015.